SPECIFIC CATION EFFECTS IN BIOLOGICAL SYSTEMS:

THERMODYNAMIC AND SPECTROSCOPIC INSIGHTS

A Dissertation

by

JAIBIR KHERB

Submitted to the Office of Graduate Studies of
Texas A&M University
in partial fulfillment of the requirements for the degree of

DOCTOR OF PHILOSOPHY

December 2011

Major Subject: Chemistry

Specific Cation Effects in Biological Systems:

Thermodynamic and Spectroscopic Insights

SPECIFIC CATION EFFECTS IN BIOLOGICAL SYSTEMS:

THERMODYNAMIC AND SPECTROSCOPIC INSIGHTS

A Dissertation

by

JAIBIR KHERB

Submitted to the Office of Graduate Studies of
Texas A&M University
in partial fulfillment of the requirements for the degree of

DOCTOR OF PHILOSOPHY

Approved by:

Chair of Committee,	Paul S. Cremer
Committee Members,	David H. Russell
	David P. Barondeau
	J. Martin Scholtz
Head of Department,	David H. Russell

December 2011

Major Subject: Chemistry

ABSTRACT

Specific Cation Effects in Biological Systems:

Thermodynamic and Spectroscopic Insights. (December 2011)

Jaibir Kherb, B.S., University of Delhi, Delhi, India

M.S., Indian Institute of Technology, Delhi, India

Chair of Advisory Committee: Dr. Paul S. Cremer

Very specific protein-salt interactions are involved in a multitude of biological phenomena such as protein folding/stability, enzymatic activity, and signal transduction events. In this work, we used two very simple, protein-mimic model biopolymers to obtain a better understanding of specific cation effects operating in aqueous protein environments. The two biopolymers used were Elastin-like Polypeptides (ELPs) and poly(*N*-isopropylacrylamide) (PNIPAM). ELPs are an especially an ideal model system as these polypeptides can be easily genetically engineered to observe the effect of specific amino acid residues and peptide chain length on these salt interactions. Both of these biopolymers are also highly thermoresponsive as their aqueous solutions undergo a hydrophobic collapse/aggregation induced phase transition process above a lower critical solution temperature (LCST). Thermodynamic measurements of these biopolymers were carried out under various salt solution conditions. Additionally, both of these biopolymers are suitable for making surface specific spectroscopic measurements. Vibrational sum frequeny spectroscopy (VSFS), a non-linear interface sensitive

spectroscopic technique, was employed here to investigate biologically relevant cation interactions which occur at peptide/protein surfaces.

First, the LCST response of a non-polar ELP and a neutral biopolymer, PNIPAM, was investigated in the presence of 12 different alkali, alkaline-earth metal and transition metal chloride salts. Even though the salt interactions for uncharged proteins are dominated by anions, subtle specific cation effects were also observed. The results followed a direct Hofmeister series for cations. Most alkali cations are excluded from the polar amide regions of proteins. More polarizable cations, however, can solvate the hydrophobic moieties and somewhat counter the salting-out effect of the chloride anion. More charged and hydrated ions like lithium and divalent cations showed a weak interaction to the amide moiety through their hydration shell.

The role of acidic amino acid residues in inducing cation specificities was investigated using an aspartate-rich ELP system. Both thermodynamic and spectroscopic data conclusively proved that the negative charge on protein surfaces is the main driving force for cation partitioning and specificity under physiological relevant concentration regimes. Apparent binding constants of carboxylate moieties with cations were determined. This is the first quantitative and thoroughly systematic study of such biologically relevant cation-carboxylate interactions prevalent in enzyme active sites and protein surfaces.

DEDICATION

To my parents, Sh.Virender Singh and Smt. Santosh Devi

ACKNOWLEDGEMENTS

First of all, I would like to thank my research advisor, Dr. Paul S. Cremer, for his continuous support, guidance and encouragement throughout the Ph.D. degree program. I also sincerely thank my committee members, Dr. David H. Russell, Dr. David P. Barondeau and Dr. J. Martin Scholtz, for their helpful suggestions and support. I am also very grateful to our collaborator, Dr. Ashutosh Chilkoti, Dept. of Biomedical Engineering, Duke University for providing the DNA plasmids used in this work.

Thanks also go to my colleagues and friends, Dr. Tinglu Yang, Dr. Wei-Ssu Liao, Dr. Yanjie Zhang, Dr. Younhee Cho, Dr. Sarah Flores, Dr. Katherine Cimatu, Dr. Xin Chen, Sean Bard, Halil Okur, Kelvin Rembert, Soyoun Hwang, Ming-Chien Li, Li Jung Chen, Jennifer Jones, and the chemistry department faculty and staff members for their valuable support, advices and cooperation during my stay at Texas A&M University.

I would also like to acknowledge my family members and close friends for their kind support and inspiring presence in my life. Thanks to Anil, Praveen, Rajbir, Amita Rana, Hameeda Begum, Sri Pooja Kondapaka, and Khadhija Baig for their immense love and support throughout this journey. Thanks also to my uncle and aunt, Sh. Meher Singh and Smt. Shakuntala Devi, for their selfless love and help. A big thanks goes to my late grandfather and grandmother, Sh. Chotu Ram and Smt. Savitri Devi, for inspiring me with their simplicity and kindness.

Finally, special thanks to my parents, Sh. Virender Singh and Smt. Santosh Devi, for their endless love, care, understanding and support.

TABLE OF CONTENTS

CHAPTER Page

LIST OF FIGURES

FIGURE Page

FIGURE Page

FIGURE Page

FIGURE Page

LIST OF TABLES

CHAPTER I

INTRODUCTION

Hofmeister series

The Hofmeister series has drawn attention from scientists in various fields for more than a century since it was first discovered by Franz Hofmeister in 1888.[1-3] Different salts were ranked in order of their efficiency to precipitate egg white proteins from aqueous solution. Later, many studies revealed that it is a recurring trend that exists in many physical and biochemical processes in aqueous solution such as colloidal assembly, protein crystallization, protein denaturation, micelle stabilization, ion-channel chemistry and enzyme activity.[4-8] The ordering of anions and cations at uncharged, colloidal and protein surfaces is as follows.[9-10]

$$CO_3^{2-} > SO_4^{2-} > S_2O_3^{2-} > H_2PO_4^- > F^- > Cl^- > Br^- > NO_3^- > I^- > ClO_4^- > SCN^-$$

$$N(CH_3)_4^+ > NH_4^+ > Cs^+ > Rb^+ > K^+ > Na^+ > Li^+ > Ca^{2+} > Mg^{2+}$$

Anions on the left of chloride are highly charged and considered kosmotropic and known to strongly salt-out proteins from the solutions. Less charge density anions on the right side of chloride, on the other hand, are chaotropic and lead to salting-in of proteins. For cationic series, sodium ion generally serves as the boundary line between a cations distinction as being kosmotropic or chaotropic. However, for cation series, more charged

---

This dissertation follows the style of *Journal of the American Chemical Society*.

and hence more hydrated species comes on the right hand side whereas less charge density species lies on left side of series. Additionally, the cation hofmeister series is not only less pronounced but also the exact order seems to be highly dependent on the identity of counter-anion, protein/colloidal solution being studied as well as other experimental conditions.[10-12] Such weaker effects are generally viewed as manifestation of weaker polarizability of cations. Actually, there is no clear understanding about how cations interact with biomacromolecules and why the influence of cations follows a specific order in all systems. This intriguing question is even more important to be investigated and answered considering widespread presence of cations in biological fluids and their important role in creating vital cell potentials, efficient signaling transduction events, and maintaining enzyme/protein structure and functions.[4-5,13]

For many decades, these salt interactions were just seen as manifestation of the effect of ions on the bulk water structure and resulting relayed effect on the dissolved biomacromolecule.[6] However, this viewpoint has been challenged by some recent experimental and theoretical findings which clearly showed that the ions do not effect the water structure beyond a few hydration shells and also, the direct ion-protein interactions should be taken into account while explaining the basic underlying mechanism.[14-16] Recently, a molecular level mechanism for these ion-specific interactions was proposed from the hydrophobic collapse of thermoresponsive polymers that includes three kinds of interactions between anions and the macromolecule and its first hydration shell.[15,17-18] Firstly, strongly hydrated anions polarize the water molecule that is directly hydrogen bonded to the amide moiety of the polymer and help the

dehydration of the polymer. Secondly, the presence of ions in solution changes the surface tension at the hydrophobic/aqueous interface and leads to salting-out of the hydrophobic portion of the polymer. Thirdly, anions may directly bind to the polymer and show a salting-in effect.

Such thermoresponsive model systems should be tested further to see if the cations interact with the proteins via the same mechanism or if there are any additional forces involved in determining their specificities observed in the biological phenomena. Jungwirth and co-workers have recently reported the specific preference of sodium ion over the potassium ion by carboxylate groups for a variety of proteins and colloid systems.[19-21] These subtle binding preferences were even hypothesized to be the main reason for presence of electric potential across living cell membranes. Some other research groups have also looked into these specific ion-pairing interactions present in salt solutions, fatty acid monolayers/micelles.[22-24] However, most of these studies are limited to few cations and detailed, systematic experimental proof of concept is lacking. Carbonyl group of amide moieties of protein backbones can also be a putative binding site for cations.[25] Its relative role in determining the overall ordering of cations in hofmeister series should also be looked at. Dispersion forces of ions have also been thought to play a key role in the hofmeister effects.[26] This study is mainly focused on improving the quantitative and qualitative understanding of these hofmeister cation effects by using very simple, methodically designed biopolymers and highly sensitive thermodynamic and surface specific spectroscopic measurements.

Model biopolymers

Effects of ions on the protein folding and stability are harder to deconvolute and quantify in the naturally occurring proteins as they have significant degree of structural and compositional complexity. Additionally, the cold denaturation temperature of most proteins is well below the room temperature. This severely limits the type of proteins and salts which can be investigated for determining the overall molecular mechanism behind such interactions. Here, in this record, we have employed two very simple biopolymers, PNIPAM and ELPs, both of which can mimic the real proteins in their structural and chemical properties.

poly(N-isopropylacrylamide) (PNIPAM)

PNIPAM is a synthetic polymer composed of n-isopropylacrylamide monomer units (Fig. 1.1a). In contrast to polypeptides, PNIPAM have an amide moiety in its side chain which makes it more accessible for any possible interaction with ions or other additives. In addition, an isopropyl group is connected to each amide moiety which imparts a significant hydrophobic character to the polymer chain. This interesting make-up of the polymer makes it an ideal system for both surface specific spectroscopic measurements as well as bulk thermodynamic techniques. An aqueous solution of PNIPAM when heated above a certain temperature undergoes hydrophobic collapse/aggregation and the solution turns cloudy.[27-28] Additionally, this lower criticial solution temperature (LCST) is fairly close to the room temperature which makes it an easier model system to probe under a wide variety of experimental conditions.

Elastin-like polypeptides (ELPs)

Elastin-like Polypeptides consists of a repeat pentapeptide unit of Val-Pro-Gly-X-Gly sequence, where X represents the guest residue which can be any amino acid except proline (Fig. 1.1b).[29-30] This polypeptide is synthesized by a very simple genetic technique, recursive directional ligation (RDL). Briefly, in this technique, the DNA sequence of the desired pentapeptide monomer is repeatedly self-ligated to get a library of oligomers from which the polypeptide of interest can be easily separated. To get an ELP with variable ratio and identity of amino acids at the guest residue site, DNA sequences corresponding to specific guest residue pentapeptides were allowed to ligate with each other to create block copolymers. Such a great control on the chemistry of complex block polymers can be used to generate ELPs of varying degree of chain length, hydrophobicity, polarity and structure.[29] All synthesized ELPs have a –SKGPG leader sequence on the N-terminal and a –WP trailer sequence on the C-terminal of the polypeptide chain. Presence of the tryptophan residue in the trailer sequence can be utilized to determine the exact concentration of ELP in the solution (Molar extinction coefficient of ELP, $\varepsilon_{280\ nm} = 5690\ M^{-1}cm^{-1}$).

Similar to PNIPAM, ELPs also undergoes phase transition from an extended, open chain to a collapsed/aggregated form when the temperature is raised above their LCST (Fig. 1.2). The LCST value of an ELP depends on its exact composition and chain length which can be genetically manipulated. However, unlike a simple polymer such as PNIPAM, ELP phase transition process involves not only aggregation and collapse of polypeptide chains but also very subtle, important changes in the overall secondary and tertiary structure.[31-37] This makes ELPs a very good protein-mimic system for understanding the effects of inorganic salts and osmolytes on the protein folding/stability.

ELP notation

ELPs are commonly named in the form $X_aY_bZ_c$-n where X, Y, Z denotes the chemical identity of the guest residues, the subscripts a, b, c specifies the ratio of those guest residues, and the symbol n represents the total number of pentapeptide repeat units. For example, wild type ELP $V_5A_2G_3$-120 is a 600 amino acid polypeptide which has 60 valine, 24 alanine and 36 glycine amino acids at the 120 available guest residue sites.

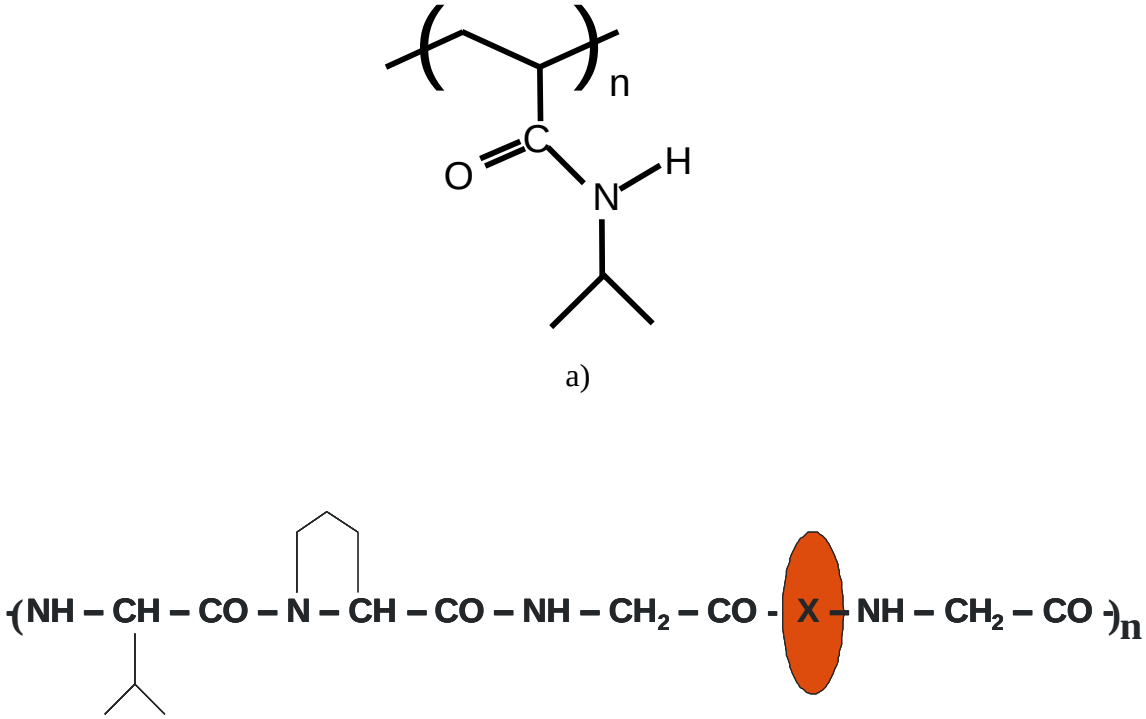

a)

b)

Figure 1.1. Chemical structure of the two biopolymers employed in this study. a) PNIPAM. b) ELPs. The orange oval shows the location of guest residue site in the ELP monomer unit.

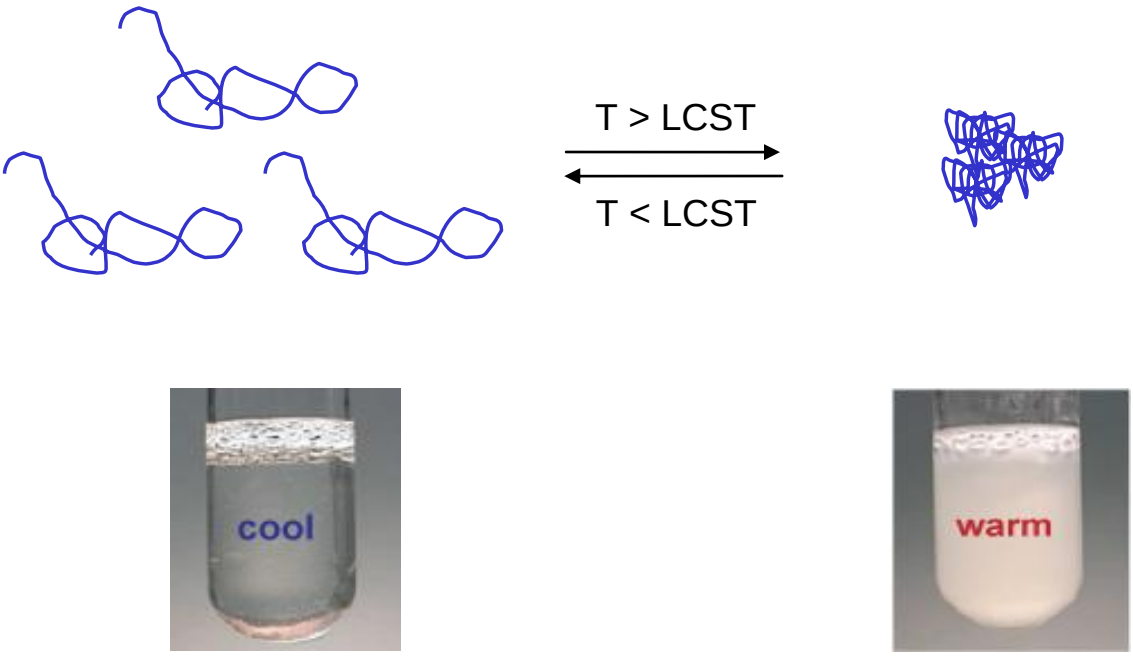

Figure 1.2. Thermoresponsive behavior of PNIPAM/ELP solutions. Above a lower critical solution temperature (LCST), these biopolymers undergo hydrophobic collapse and aggregation resulting into cloudy solution.

ELP expression and purification

The DNA gene corresponding to the desired ELP sequence was inserted into a pET expression vector.[29] The vector also contained an ampicillin resistant gene. These expression vectors were then transformed into *E. coli* strain BLR/DE3. Cells were expressed in an ampicillin containing media for 24 hrs. ELP containing cells were lysed using the sonication followed by removal of cell debris. Treatment of the resulting supernatant with poly(ethyleneimine) led to selective precipitation and removal of nucleic acids (RNA/DNA). Finally, ELP mixed with other cellular peptides was separated using a series of inverse transition cycling (ITC) steps. In short, ELP containing solution was heated to a high temperature (above its LCST value). Selectively precipitated ELP was collected by centrifugation and the resulting pellet was redissolved in cold buffer solution. A very high purity final ELP pellet was obtained when series of such hot and cold temperature cycles were performed. The overall schematic of this ELP preparation process is shown in Fig. 1.3.

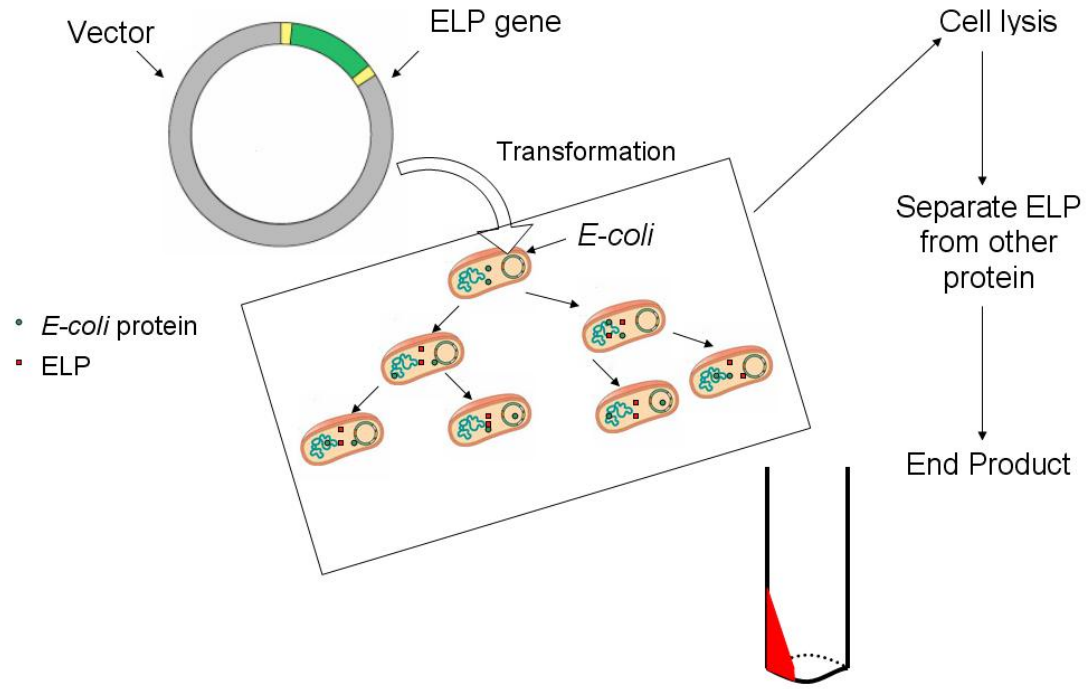

Figure 1.3. Schematic diagram showing the ELP preparation and purification. [29-30]

Dynamic light scattering instruments

The thermodynamic response of both of these temperature sensitive biopolymers were recorded as a function of different solution conditions (pH, salt concentrations, chemical nature of salts) using dynamic light scattering instruments. Based on the sample requirements and the desired temperature range of individual experiments, two different instruments were used for light scattering measurements.

Linear temperature gradient device

Our laboratory-made temperature gradient device was used for collecting light scattering data of biopolymer solutions (Fig. 1.4).[15,17] It consists of two brass tubes (1/8 " width, K& S Engineering, Chicago, IL) fixed parallel to each other. A hot antifreeze solution was flowed through one tube while a cold antifreeze solution was flowed the other tube, resulting into the formation of a linear temperature gradient across the small separating distance of 5 mm between the tubes. A glass cover slip was mounted on the top of two brass tubes as a sample stage. Six rectangular borosilicate capillary tubes (dimensions: 2 cm length × 1 mm width × 100 μm height) filled with desired aqueous polymer/peptide solution were placed on the sample stage (Fig. 1.4).

The light scattering images of the thermoresponsive sample solutions were recorded via a CCD camera using dark field optics under an inverted microscope (Fig. 1.5). A line scan was drawn across each capillary tube image to determine the exact position of phase transition process (Fig. 1.6). Comparing this data with the images of two standard polymer or organic samples (with known LCST/Melting point values), this position information was easily converted to determine the exact temperature at which different samples underwent phase transition. For this purpose, in each measurement, two capillary tubes containing known LCST value standard organic/polymer solutions were placed alongside four capillary tubes of ELP/PNIPAM samples so as to calibrate the temperature gradient. High throughput of capturing phase transition images as well as low sample quantity requirements (2-3 μL per capillary tube) makes it a very useful tool for such measurements. Additionally, this device have the capability to observe the kinetics of more complex phase transition processes such as aqueous two-phase system commonly observed in protein crystallization processes.

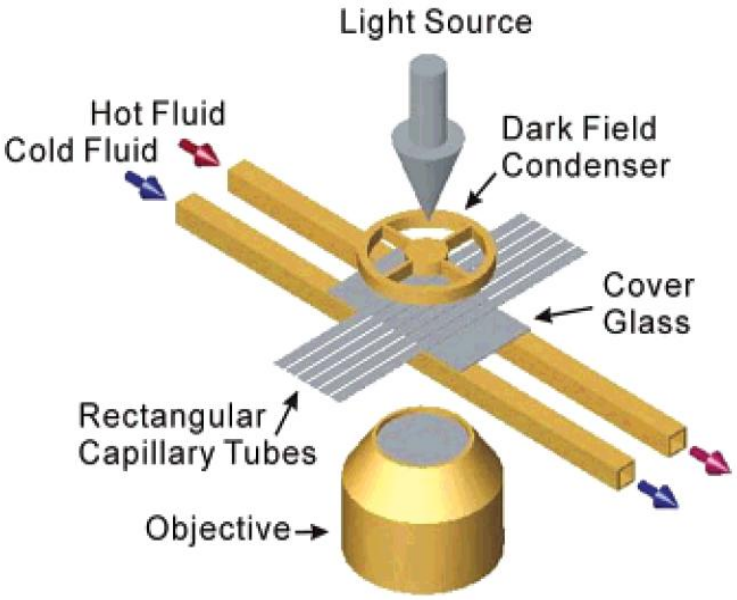

Figure 1.4. Schematic diagram of linear temperature gradient device used for dynamic light scattering measurements.

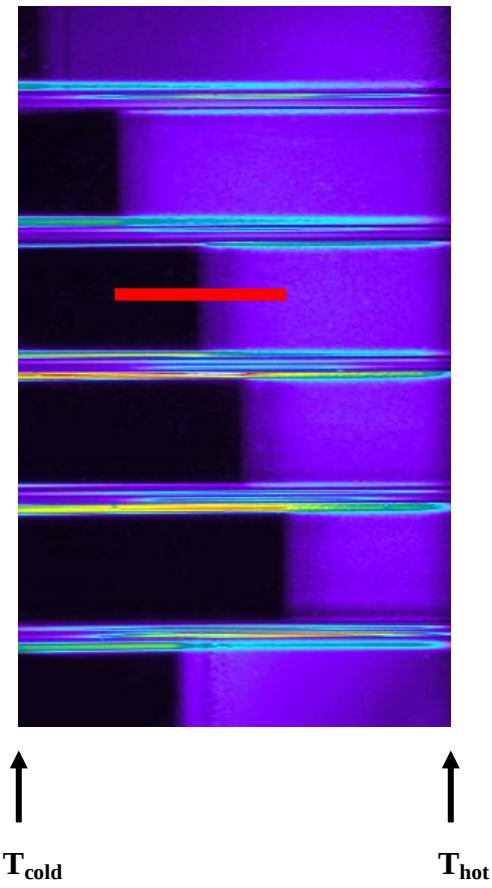

Figure 1.5. A dark field microscopic image of 6 capillary tubes undergoing the phase transition process on temperature gradient device. Capillary tubes 1 and 6 were filled with known LCST samples of PNIPAM solutions in 0.7 M KCl and 0.35 M KCl respectively. Capillary tubes 2 to 5 were filled with 10 mg/ml solution of V_5-120 ELP in 0.3 M NaCl, 0.1 M NaCl, 0.05 M NaCl, and 0.0 M NaCl, respectively. The exact phase transition temperature was determined by drawing a line scan across the phase transition region (as shown for capillary tube 3).

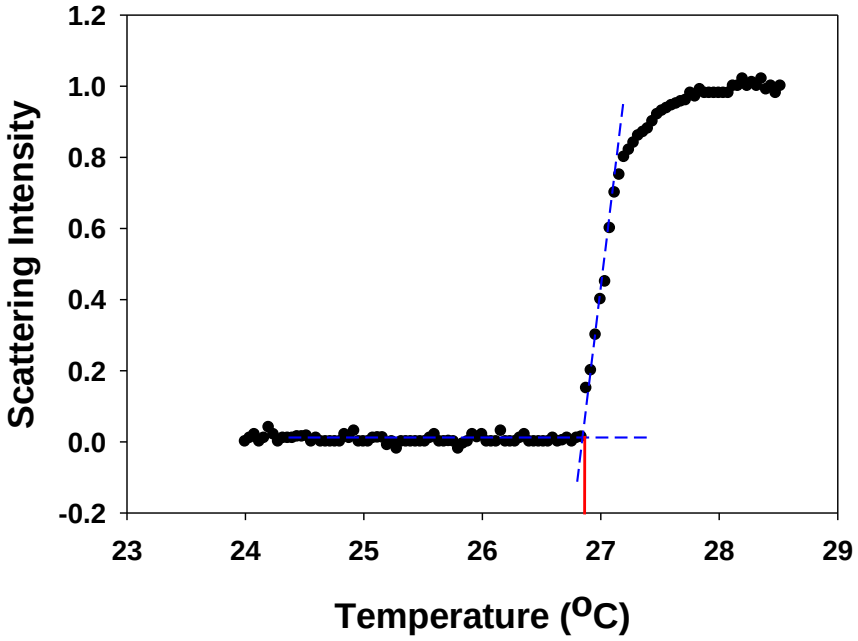

Figure 1.6. Line scan profile of the straight red line drawn in Fig. 1.5. Two dashed blue lines are drawn through the data below and just above the phase transition process. The intersection of these two lines is taken as the LCST value. This onset point is shown by the red vertical line.

Melting point apparatus, MPA 100

A more conventional and simpler melting point system, OptiMelt^{TM} MPA 100 (Stanford Research Systems), was also employed for taking LCST data (Fig. 1.7a.). In a typical LCST measurement, three capillary tubes filled with identical ELP/PNIPAM solutions were placed in the heating chamber of the melting point device. The samples were then subjected to a gradual temperature ramp and the light scattering intensity of the samples was recorded as a function of temperature (Fig. 1.7b). The ramping rate of heating can be easily adapted from 0.1 ^{o}C/min to 20 ^{o}C/min depending on the requirement of a particular experiment. The in-built camera on the instrument captured real-time images of the samples and then used digital image processing to determine the onset of the LCST. The real time scattering data was automatically recorded by the meltview software. This instrument requires only 5-10 μL sample volume per capillary tube. As compared to linear temperature gradient device which was described earlier, OptiMelt^{TM} gives the absolute value of the phase transition temperature. In addition, this device can also be operated in a much wider temperature range (~ 5 ^{o}C to 400 ^{o}C).

a)

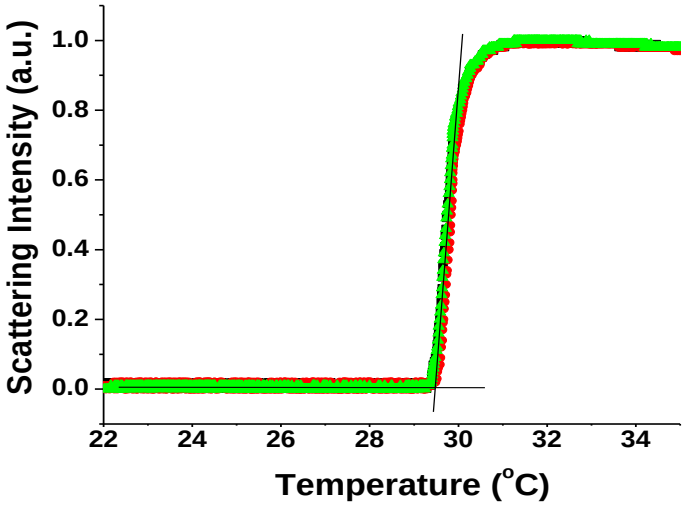

b)

Figure 1.7. a) Automated melting point apparatus, OptiMelt™ MPA 100 (Stanford Research Systems).[38] b) Phase transition process of 10 mg/ml PNIPAM in 200 mM NaCl as observed by melting point apparatus. Green, red and black curves shows the simultaneous recording of scattering data from three capillary tubes. Two black lines are drawn through the scattering data to show the exact onset point.

Vibrational sum frequency spectroscopy (VSFS)

VSFS is a second-order nonlinear spectroscopic technique in which two input beams with frequencies ω_{IR} and ω_{VIS} are overlapped temporally and spatially to generate an output beam at the sum frequency, ω_{SFG} (Fig. 1.8).[39-41]

$$\omega_{SFG} = \omega_{IR} + \omega_{VIS} \tag{1.1}$$

ω_{IR} is the frequency of input infrared (IR) beam whereas ω_{VIS} is the frequency of input visible beam. The intensity of this sum frequency beam, I_{IR}, is directly proportional to the intensity of the two input infrared and visible beams, I_{IR} and I_{VIS}, and the square of effective second-order nonlinear susceptibility, $\chi_{eff}^{(2)}$ (eqn. 1.2).

$$I_{SFG} \propto \left|\chi_{eff}^{(2)}\right|^2 \bullet I_{vis} \bullet I_{IR} \tag{1.2}$$

This second-order non-linear susceptibility tensor can be further expressed in terms of resonant and nonresonant contributions in the sum frequency signal (eqn. 1.3).

$$\chi_{eff}^{(2)} = \chi_{NR}^{(2)} + \chi_{R}^{(2)} = \chi_{NR}^{(2)} + \sum_{v} \frac{A_v}{\omega_{IR} - \omega_v + i\Gamma_v} \tag{1.3}$$

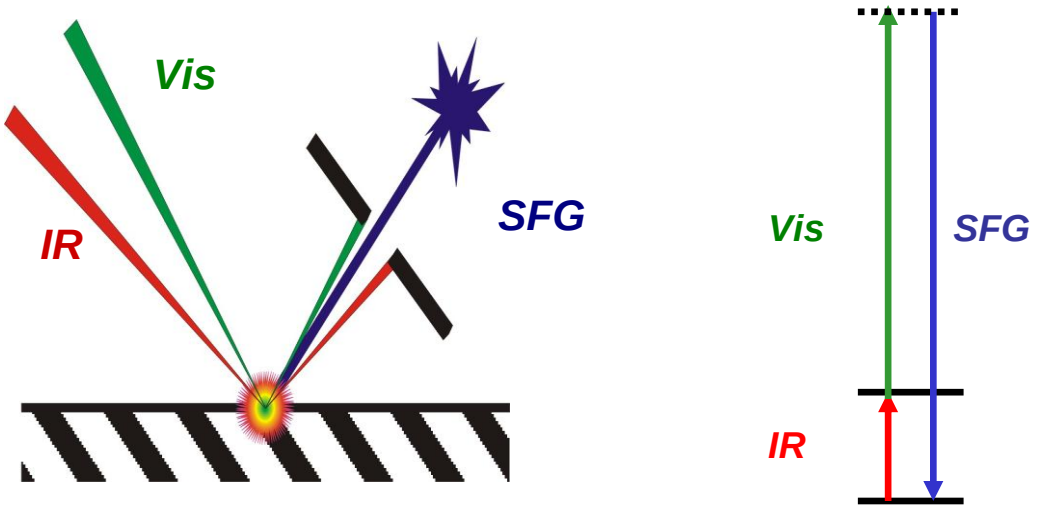

a) b)

Figure 1.8. Schematic diagram showing the principle of vibrational sum frequency spectroscopy (VSFS). a) Temporal and spatial overlapping of input infrared and visible beams at the sample surface to generate the sum frequency signal beam. b) Sum frequency beam is a linear combination of input infrared and visible beams.

$\chi_R^{(2)}$, $\chi_{NR}^{(2)}$ are the resonant and nonresonant second order nonlinear susceptibilities terms. ω_v is the vibration frequency, A_v is oscillator strength and Γ_v is the peak width of the vibrational transition.

Because of the unique vibrational selection rules involved in the sum frequency process, this technique does not give any signal for media or samples having complete inversion symmetry of molecules. However, this technique is a very sensitive probe for monitoring surfaces and interfaces which inherently lacks inversion symmetry. When the frequency of input IR beam is in resonance with a particular vibrational mode in an inversion symmetry lacking system, an enhancement in the sum frequency signal is observed. As a result, surface specific chemical information of molecules including their relative abundance and conformation can be obtained without worrying about the interference coming from bulk of the solutions.[39] This is clearly the biggest advantage of employing this nonlinear vibrational spectroscopy over the traditional spectroscopy techniques such as fourier transform infrared spectroscopy (FTIR). VSFS has already been shown to provide helpful information about air/water, organic/water, solid/water, lipid membranes/water and protein/water interfaces.[41-45]

Instrumental set-up

A passive/active mode locked Nd:YAG laser (PY61C, Continuum Inc., Santa Clara, CA) equipped with a negative feedback loop in oscillator cavity was employed to generate the fundamental 1064 nm laser beam. The laser beam produced by this cavity dumping technique had a pulse width of 17 picoseconds and had a very high shot-to-shot

stability and beam uniformity. The laser pulse repetition rate was 20 Hz and energy of the generated beam was 50 mJ/pulse.

The fundamental 1064 laser beam was then sent to an optical parametric generator/amplifier (OPG/OPA) stage system ((LaserVision, Bellevue, WA).[46] Firstly, the horizontally polarized 1064 nm beam was divided into two parts by a beamsplitter and sent into two different beam paths. One beam was frequency doubled to provide the 532 nm input light for angle-tuned down conversion stage of OPG/OPA process. This first stage consisted of two potassium titanyl phosphate (KTP) nonlinear crystals. This resulted in generation of idler beam of frequency 1.35 to 1.85 μm. This output idler beam was then combined with path delayed fundamental 1064 nm beam at an angle-tuned potassium titanyl arsenate (KTA) stage. The exact positions of nonlinear crystals at KTP/KTA stages were easily controlled by Microsoft Windows^{TM} based software program. This overlapping process produced tunable infrared beam in 2000-4000 cm^{-1} region. The intensity of this generated IR beam was close to 600 μJ/pulse at 3200 cm^{-1}.

The tunable IR beam was overlapped temporally and spatially with the 532 nm radiation at the sample stage by guiding the two beams through appropriate stearing optics, focusing lenses and polarizers (Fig. 1.8). The resulting sum frequency signal containing information from the sample surface was collected by a photomultiplier tube (Hamamatsu, Japan). This recorded signal was then sent to a gated boxcar integrator and the data was recorded digitally. All the vibrational spectra reported in this study were taken with ssp (s-sum frequency, s-visible and p-infrared) polarization combination of the input and output beams.

Spectral regions of interest

In our VSFS studies of biopolymer interfaces, we focused on the spectral features and changes which occur in 2800-3750 cm^{-1} region. The –CH stretching frequencies arising from alkyl/nonpolar groups of PNIPAM/ELP were present in 2800-3100 cm^{-1} part of the spectrum whereas –OH stretching arising from interfacial water molecules or OH groups were located in 3200-3700 cm^{-1} region. A representative spectrum of pure deionised water at air-water interface is shown in Fig. 1.9. Three prominent spectral features can be clearly seen in this VSFS spectrum. A broad band centered around 3200 cm^{-1} is normally assigned to tetrahedrally coordinated water molecules (commonly referred to as the water molecules with "ice-like" structure). The peak around 3400 cm^{-1} comes from less ordered water molecules having "liquid-like' coordinated structure. At high frequency, a sharp and strong peak near 3700 cm^{-1} can also be observed which is generally ascribed to free dangling –OH groups at the interface.[41] In the presence of any surface active species such as hydrocarbons/surfactants/membranes/proteins, disappearance of this free –OH peak serves as a signature for confirming the formation of a good Gibbs/Langmuir monolayer at the interface.

In this study, systematic VSFS investigations of biopolymer interfaces were carried out in the presence of diverse set of experimental conditions. The changes in the spectral features in –OH and –CH regions can provide very vital information about sensitive yet very critical interactions occurring at the protein/peptide interfaces.

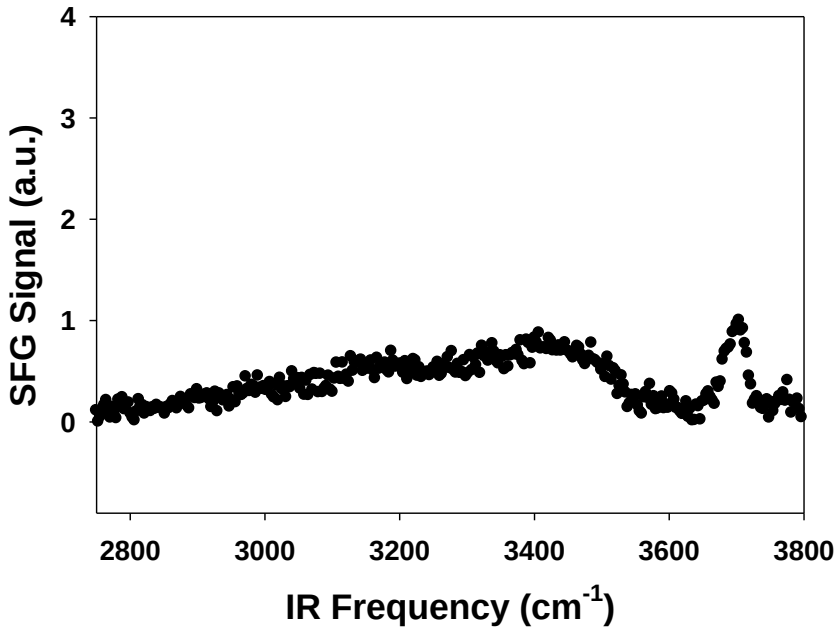

Figure 1.9. VSFS spectrum of an air-water interface taken with deionised water and ssp polarization combination. Distinct –OH vibrational bands can be seen in 3200-3700 cm^{-1} region.

CHAPTER II

THE MECHANISM FOR SPECIFIC CATION EFFECTS ON THE HYDROPHOBIC COLLAPSE OF NEUTRAL BIOPOLYMERS (ELASTIN-LIKE POLYPEPTIDES OR PNIPAM)

Introduction

Herein, phase transition temperatures of a nonpolar elastin-like polypeptide and poly(*N*-isopropylacrylamide) were measured in the presence of a series of alkali, alkaline earth metal and other biologically relevant metal chloride salts solutions. Relative quantitative efficiencies of these cations to salt-out these neutral protein-mimics were determined. It was observed that the trends followed general hofmeister series and showed linear dependence with increasing concentration of salts. The underlying forces behind these subtle cation effects were elaborately explained and summarized in terms of physical paramteres of ions such as their polarizibilities, hydrophobicities, hydration properties and preferences for particular functional motifs on the dissolved biopolymer.

More specifically, the hydrophobic collapse of a neutral elastin-like polypeptide (ELP) and poly(*N*-isopropylacrylamide) (PNIPAM) is employed for elucidating the mechanism for hofmeister cation series. PNIPAM is composed of monomer units of isopropylacrylamides (Fig. 2.1b). Presence of both hydrophilic (amide group) and hydrophobic group (isopropyl moiety) in its side chain make it an interesting candidate to study protein denaturation and specific ionic effects.[15,17,47-48] PNIPAM becomes insoluble above its lower critical solution temperature and starts scattering light (Chapter I).[27-28] This phenomenon is generally attributed to hydrophobic aggregation or collapse

of polymer chains. ELP (Elastin-like polypeptides) is the second model system employed in this study. ELPs consist of a pentapeptide repeat unit Val-Pro-Gly-Xaa-Gly, where Xaa can be any amino acid except proline (Chapter I). The chain length and guest residue identity in these peptides can be easily controlled and manipulated during the genetic engineering process.[29-30,49] Herein, V_5-120 ELP was used in the experimental studies. It consists of 120 repeat units of –VPGVG- sequence (Fig. 2.1b). ELPs also undergo phase transition above their LCST which is generally close to room temperature. However, unlike PNIPAM, aggregation or phase separation of ELPs also involves significant β-turn/β-spiral secondary/tertiary structure formation.[31-37] It should be noted that the two model systems used here should be able to provide complimentary information because PNIPAM have amide moiety in the side chain whereas ELP have it in the main back-bone just like proteins and peptides. Additionally, PNIPAM and V_5-120 ELP contain hydrophobic isopropyl groups and hydrophobic amino acid residues respectively in their polymeric chains. Lack of any charged moieties helps in deconvoluting and understanding the salt effects more effectively. Use of such systems will lead to an improved understanding of ionic interactions with amide/hydrophilic moieties and hydrophobic groups during the protein denaturation and precipitation process. This is especially important since most of the naturally occurring proteins consist of complex secondary/tertiary structures and varying degree of charged/hydrophobic residues which makes these concurrently occurring specific cation interactions effects hard to decipher and observe.[5-6]

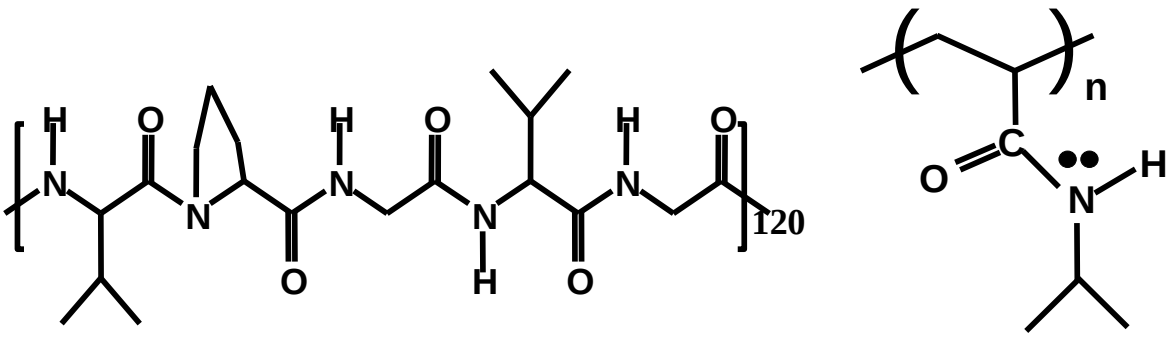

a) b)

Figure 2.1. Structure of the biopolymers used in the study. a) V_5-120 ELP. b) PNIPAM.

Experimental

ELP preparation

V_5-120 ELP was employed as the model system in the study. This polypeptide consists of 120 pentapeptide repeat units of amino acid sequence –VPGVG-. pET plasmids of this particular genetic sequence were constructed using recursive directional ligation (RDL) process. This strategy of making oligomers of a particular amino acid sequence is described previously (Chapter I).[29] Resulting plasmids were transformed into BLR/DE3 E.*coli* cells and the ELP plasmid containing cells were expressed for 24 hrs in ampicillin supplemented high nutrient growth media (TB Dry^{TM}). Cells were centrifuged and resuspended in 10 mM, pH 7.1 buffer followed by cell lysis using sonication (Sonicator® 3000 system; Mandel scientific company Inc.). Polyethyleneimine treatment of supernatant was done to remove nucleic acids from cell lysate. ELP was purified from other cell lysates and proteins using a series of 'inverse transition cycling' steps. In short, ionic strength of supernatant was increased by adding 2 M NaCl and solution was heated above the phase transition temperature of V_5-120 ELP. This leads to the separation of ELP from other impurities. ELP pellet, after centrifugation, was redissolved in cold buffer and heated again for further purification. The molecular weight and purity of obtained ELP was confirmed by typical SDS-PAGE and $CuCl_2$ staining method. Finally, ELP dissolved in buffer was dialyzed against purified deionized water. The concentration of purified ELP in dialyzed solution was determined by measuring the absorbance at 280 nm (ε = 5690 $M^{-1}cm^{-1}$ for ELP). For further usage in thermodynamic measurements, ELP samples were lyophilized and stored at – 80 ^{o}C.

PNIPAM synthesis and purification

PNIPAM (poly(*N*-isopropylacrylamide)) was synthesized by free radical polymerization of its monomer, N-isopropylacrylamide. In brief, a solution of N-isopropylacrylamide and 2, 2'- azoisobutylnitrile (AIBN) in methanol was lowered into a pre-heated oil-bath at 70^{o} C under positive pressure of N_2. After 25 hrs of reaction time, a solid product was separated by evaporating the solvent. The polymer was separated from unreacted monomer by redissolving in acetone and then precipitating the polymer in hexane three times. The purified product had four fractions with molecular weights of 4.75×10^5, 1.7×10^5, 5.58×10^4, 1.78×10^4 g/mol as noted by static light scattering measurements in methanol. The 1.78×10^4 g/mol fraction was used for all the measurements in this study.

High purity inorganic salts NaCl, KCl, LiCl, CsCl, RbCl, NH_4Cl, NMe_4Cl, $CaCl_2$, $BaCl_2$, $SrCl_2$, $MgCl_2$, and $ZnCl_2$ were purchased from Sigma Aldrich (> 99 % purity). Low conductivity deionised water, obtained from a NANOpure Ultrapure water system (minimum resistivity of 18 MΩ.cm), was used to prepare all the salt solutions. V_5-120 ELP and PNIPAM were dissolved in respective salt solutions to get a final polypeptide/polymer concentration of 10 mg/ml. The phase transition temperature measurements were taken with an automated melting point apparatus (Optimelt^{TM} MPA 100, Stanford Research Systems). Ramping rate of 0.5 ^{o}C/min was used in all the measurements. In a typical LCST measurement, three capillary tubes filled with desired ELP solution in a particular salt was placed in the heating chamber of the melting point device and scattering intensity of samples were recorded as a function of change in

temperature. The in-built camera of instrument captured real-time images of the samples and then use digital image processing technology to determine their phase transition temperatures. All LCST values reported in this study are highly repeatable and the shown data is an average of six measurements.

Results

LCST data of V_5-120 ELP with various chloride salts

Firstly, LCST values of V_5-120 ELP were recorded in the presence of increasing concentration of various monovalent chloride salts (Fig. 2.2). Chloride salts of Li^+, Na^+, K^+, Rb^+, Cs^+, NH_4^+ and NMe_4^+ were tested for this purpose. The aqueous solution of this hydrophobic ELP undergoes phase transition close to 28.5 ^oC. In total, seven monovalent cations were tested covering wide range of ionic size, polarity and hydrophobicity. As expected, gradual linear decrease in the phase transition temperature was observed with increasing concentration for all monovalent salts. Interestingly, ELP solubility was found to depend significantly on the chemical identity of cationic species and the efficiency of a cation to salt-out ELP from solution followed direct hofmeister series.

$$Na^+ > K^+ > Rb^+ > Cs^+ > NH_4^+ > Li^+ > NMe_4^+$$

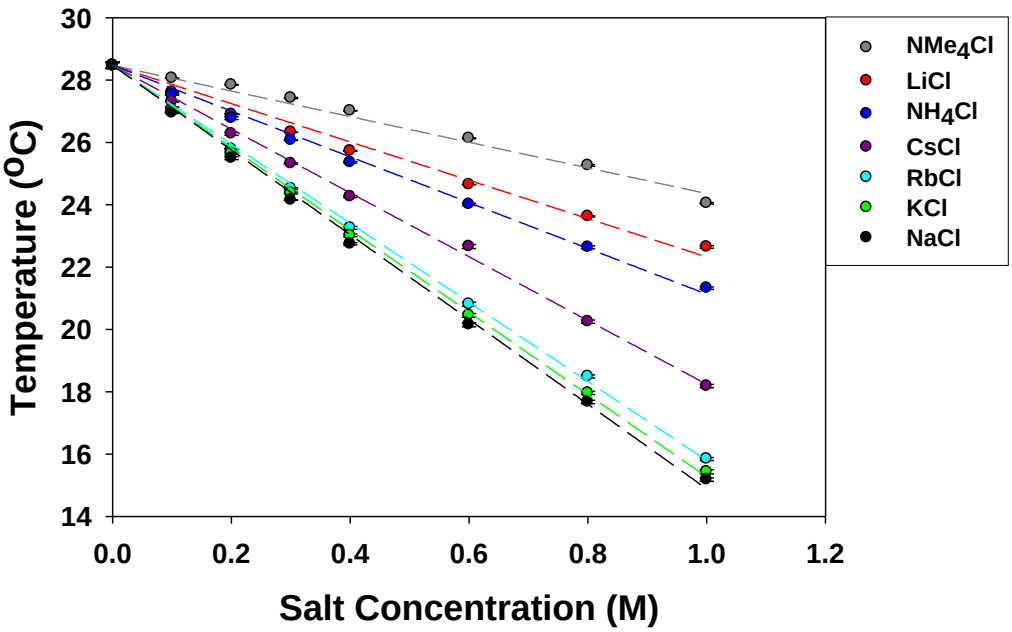

Figure 2.2. LCST values of V_5-120 ELP in the presence of increasing concentration of monovalent chloride salts. All measurements were done with 10 mg/ml ELP concentration. Each data point represents an average of six measurements and the associated experimental standard deviations are within the size of circles used to plot the data. The dashed lines are fits to equation 2.1.

Corresponding data was also taken with multiple alkaline-earth and transition metal ions (Fig. 2.3). Divalent ions also caused a linear decrease in ELPs LCST and the data fitted fairly well with eqn. 2.1. The salting out efficiency of divalent cations is significantly smaller than the monovalent cations especially after considering the fact that for the same concentration of salt, divalent metal chloride solutions contain twice the number of chloride anions. These ions were tested so as to increase the scope of understanding the effect of an ion's charge, hydration property and its relative hofmeister effect on the biomacromolecule solvation and stability. The salting-out order of divalent ions was found to be:

$$Zn^{2+} > Ba^{2+} > Sr^{2+} > Mg^{2+} > Ca^{2+}$$

Additionally, LCST value of this fully hydrophobic ELP was found to be fairly constant irrespective of the solution pH (Fig. 2.4). Henceforth, any effect of salt-specific pH changes on LCST values can be neglected.

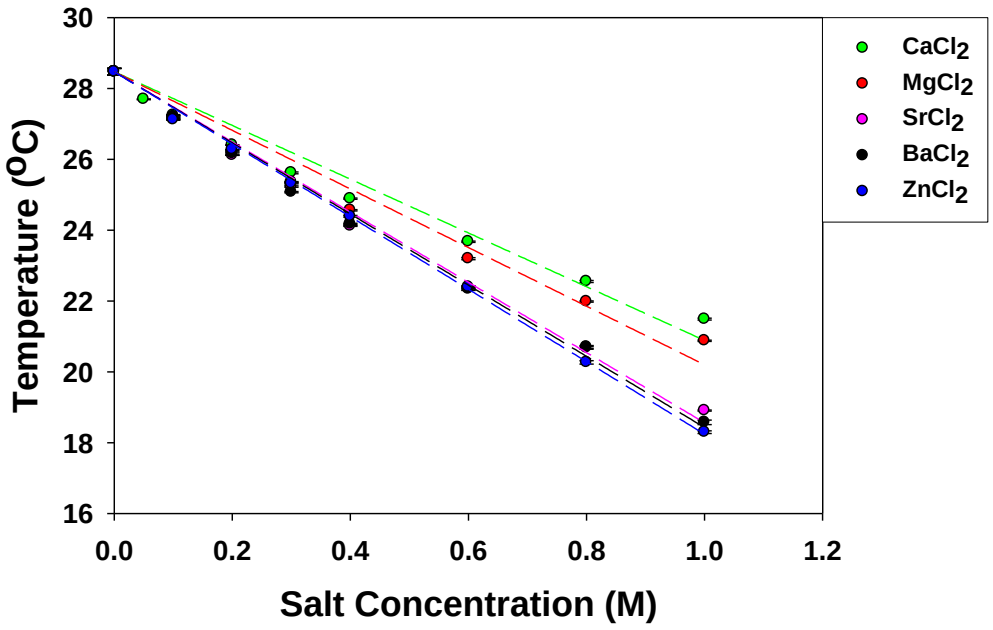

Figure 2.3. LCST values of V_5-120 ELP in the presence of increasing concentration of divalent chloride salts. All measurements were done with 10 mg/ml ELP concentration. Each data point represents an average of six measurements and the associated experimental standard deviations are within the size of circles used to plot the data. The dashed lines are fits to equation 2.1.

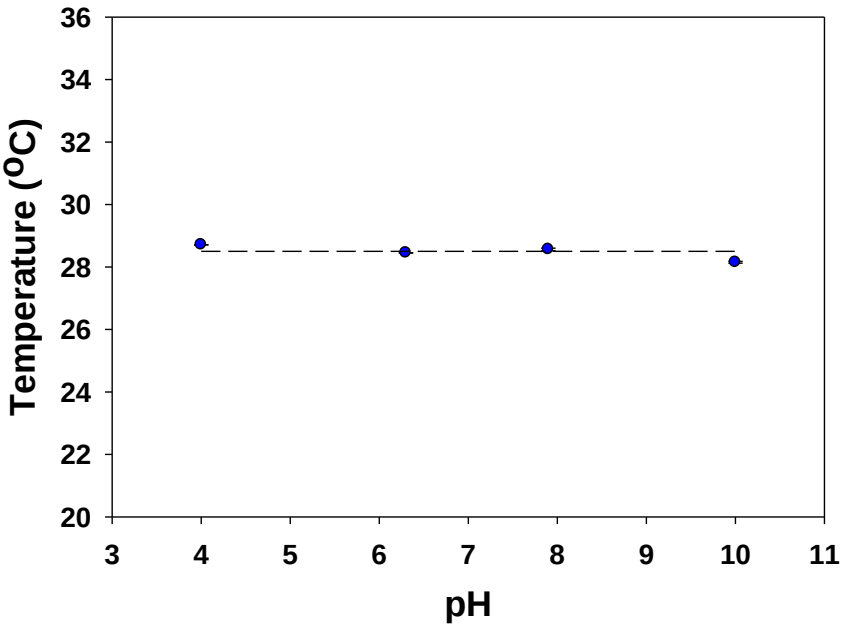

Figure 2.4. LCST values of V_5-120 ELP as a function of solution pH. All measurements were done with 10 mg/ml ELP concentration. pH was adjusted by adding concentrated HCl/NaOH. Each data point represents an average of six measurements and the standard deviations are within the size of circles used to plot the data.

LCST data of PNIPAM with various chloride salts

Another hydrophobic biopolymer with a more accessible amide moiety needed to be tested to compliment and compare the results obtained from a simple hydrophobic polypeptide such as V_5-120. PNIPAM was chosen for this purpose. All other experimental conditions were kept completely identical. This interesting thermoresponsive biopolymer has amide group and isopropyl group in its chain. LCST values of an aqueous solution of PNIPAM were recorded in the presence of increasing concentration of seven different monovalent chloride salts (Fig. 2.5). The salting out efficiency of the tested monovalent ions was found to follow this order.

$$Na^+ > K^+ > Rb^+ \sim Cs^+ > NH_4^+ > Li^+ > NMe_4^+$$

Divalent metal ions also showed significant differences in their ability to effect the solubility of PNIPAM (Fig. 2.6). The relative order of salting-out PNIPAM from the solution was found as follows.

$$Ba^{2+} > Sr^{2+} > Zn^{2+} > Ca^{2+} > Mg^{2+}$$

Similar to ELP, PNIPAM also showed negligible response to any pH changes in solution (Fig. 2.7). This conclusively proves the role of specific cation effects behind these subtle observed differences in LCST values rather than any manifestation of salt induced pH change.

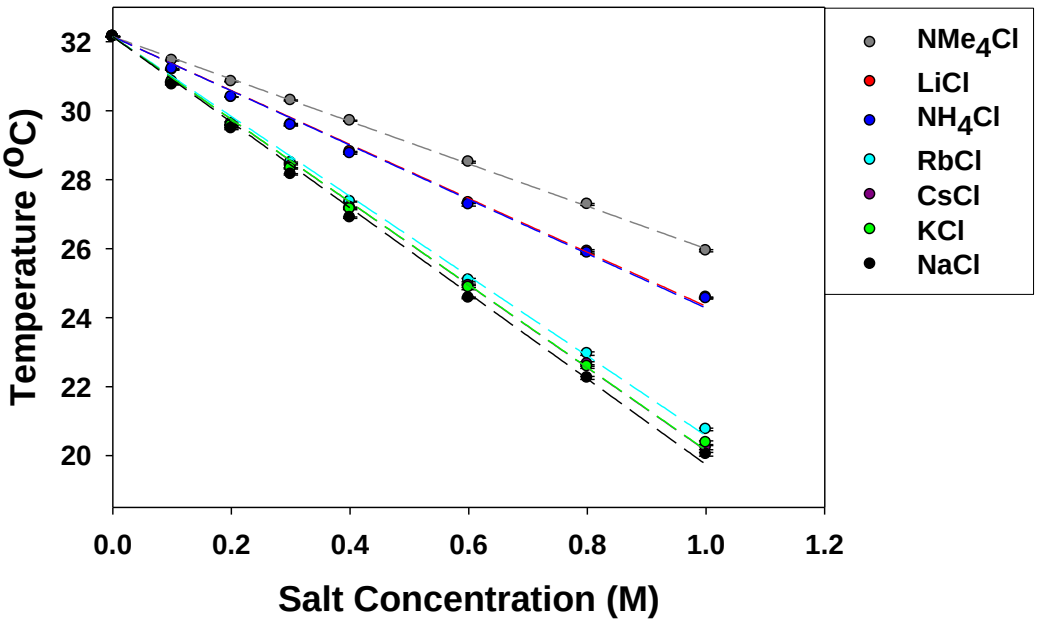

Figure 2.5. LCST values of PNIPAM in the presence of increasing concentration of monovalent chloride salts. All measurements were done with 10 mg/ml PNIPAM concentration. Each data point represents an average of six measurements and the associated experimental standard deviations are within the size of circles used to plot the data. The dashed lines are fits to equation 2.1.

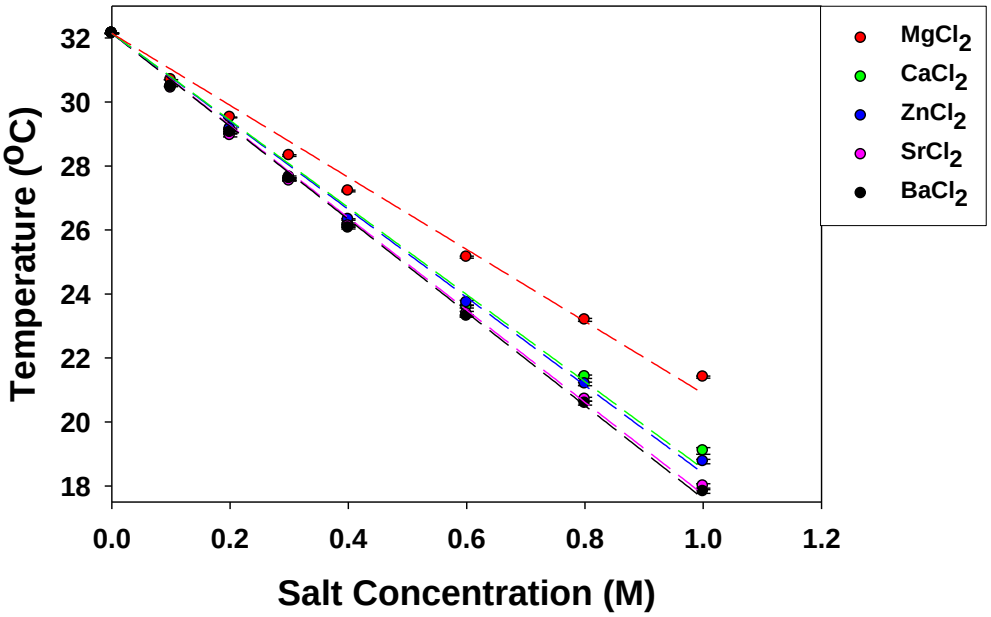

Figure 2.6. LCST values of PNIPAM in the presence of increasing concentration of divalent chloride salts. All measurements were done with 10 mg/ml PNIPAM concentration. Each data point represents an average of six measurements and the associated experimental standard deviations are within the size of circles used to plot the data. The dashed lines are fits to equation 2.1.

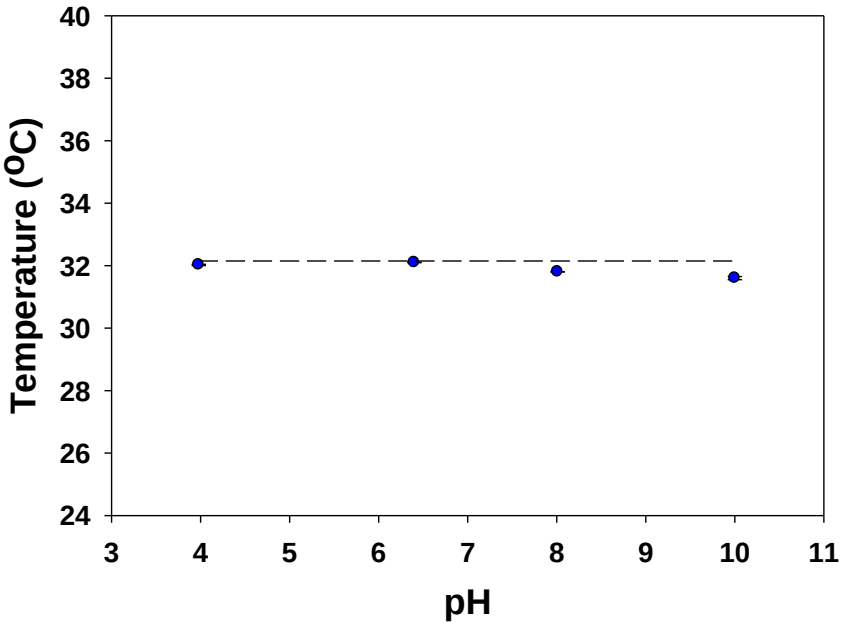

Figure 2.7. LCST values of PNIPAM as a function of solution pH. All measurements were done with 10 mg/ml polymer concentration. pH was adjusted by adding concentrated HCl/NaOH. Each data point represents an average of six measurements and the standard deviations are within the size of circles used to plot the data.

Data fitting

The phase transition data for both V_5-120 ELP as well as PNIPAM can be fitted by a simple linear equation.

$$T = T_0 + c[\mathrm{M}] \tag{2.1}$$

where T_0 is the phase transition temperature of ELP in deionised water; [M] is the molar concentration of salt, and c is a constant with units of temperature/molarity.

Previously, the phase transition temperature data of hofmeister anions with these two biopolymers had been fitted successfully with a similar equation, which consisted of a constant, a linear term and a Langmuir binding isotherm (eqn. 2.2).[15,18]

$$T = T_0 + c[M] + \frac{B_{\max} K_A [M]}{1 + K_A [M]} \tag{2.2}$$

where T_0 is the LCST of polymer/polypeptide in the absence of salt. [M] is the molar concentration of salt and c is a salting-out term having units of temperature/molarity. K_A is the apparent binding constant of each specific anion to the polymer and $B_{\max}$, a constant having the units of temperature, is the increase in phase transition temperature of polymer due to direct anion binding at a saturation salt concentration. Overall, the effects of specific hofmeister anions were quantified and correlated in terms of surface tension increment, polarization of interfacial water, and direct ion binding tendencies of

each individual anion.[15] However, the LCST data for cations shown here doesn't seem to have any significant direct ion binding curvature in their trends, atleast not with the salt concentrations which were employed in the experiments. So, the thermodynamic data was fitted with a simple linearly decreasing term (eqn. 2.1). The *c* values obtained from fittings were normalized (c_{NaCl} was taken as reference) and ionic strength variations for bivalent salts were taken into account.

$$c_{monovalent} = c - c_{NaCl} \tag{2.3}$$

$$c_{divalent} = c - 2c_{NaCl} \tag{2.4}$$

Sodium chloride was taken as reference as the constituent ions Na^+ and Cl^- comes right in the middle of hofmeister series for cations and anions respectively.[6] Table 2.1 shows the obtained fitted values for both PNIPAM and V_5-120 ELP.

Table 2.1. Fitted values of parameter *c* obtained by plotting LCST data of PNIPAM and V_5-120 ELP with 12 different chloride salts using equation 2.1.

Salt	**PNIPAM**		**V_5-120 ELP**	
	c **(^{o}C/mol)**	**Normalized value of *c** (^{o}C/mol)**	***c*** **(^{o}C/mol)**	**Normalized value of *c** (^{o}C/mol)**
LiCl	-7.82 ± 0.22	4.59	-6.15 ± 0.3	7.44
NaCl	-12.4 ± 0.25	0	-13.6 ± 0.27	0
KCl	-12 ± 0.19	0.42	-13.2 ± 0.16	0.38
RbCl	-11.6 ± 0.18	0.84	-12.7 ± 0.15	0.91
CsCl	-12 ± 0.16	0.41	-10.2 ± 0.18	3.36
NH_4Cl	-7.87 ± 0.22	4.54	-7.34 ± 0.2	6.25
NMe_4Cl	-6.15 ± 0.06	6.26	-4.11 ± 0.21	9.48
$MgCl_2$	-11.3 ± 0.43	13.6	-8.27 ± 0.61	18.9
$CaCl_2$	-13.6 ± 0.48	11.2	-7.6 ± 0.51	19.6
$BaCl_2$	-14.5 ± 0.22	10.3	-10 ± 0.30	17.1
$SrCl_2$	-14.4 ± 0.28	10.4	-9.91 ± 0.35	17.3
$ZnCl_2$	-13.8 ± 0.33	11.1	-10.2 ± 0.17	16.9

* c_{NaCl} was taken as reference for normalization.

Discussion

Salting-out and salting-in behavior of proteins and other biopolymers is generally dominated by the interactions with the anionic species of hofmeister salts.[4,10] Even in this work, greater contribution of chloride species on the overall LCST decrease can be clearly seen. Infact, both ELP and PNIPAM showed linear decrease in LCST with all chloride salts irrespective of the counter-cation being kosmotropic or chaotropic (Figs. 2.2, 2.3, 2.5 and 2.6). No significant salting-in curvature was observed with any studied salts at low concentrations. This result is on the expected line since many spectroscopic and theoretical studies have shown that most of the alkali cations are excluded from air-water or polymer-water interfaces.[50-55] It should also be noted here that the increment of surface tension by salt addition is primarily governed by the identity of anion, not cation (Table 2.2).[56-57] Therefore, surface tension could not possibly be the differential force in these subtle cation specific induced decreases observed in phase transition temperatures.[58]

Many theories have been used in the past to describe the salts effects on the solubility of non-polar compounds and gases in salt solutions. Initially, these interactions were thought to be simply due to electrostatic effect of added salts and related changes in the dielectric constant of water.[59] But, it failed to explain the observed specific ion effects for the same ionic strength salt solutions and hence this notion of salt effects was soon challenged by other viewpoints.[60] Internal pressure theory proposed by Long and Mcdevit gave very good qualitative predictions of these salt effects for a vast variety of hydrocarbons.[60-61] Salt effects were viewed in terms of the volume change of water when

Table 2.2. Literature values of hydration entropy of different cations and surface tension increments observed in their respective chloride salt solutions.[57]

Ion	**Hydration entropy (J/K mol)**	**Δσ* (mN L/m mol)**
Li^+	-142	1.63
Na^+	-111	1.64
K^+	-74	1.4
Rb^+	-65	1.56
Cs^+	-59	1.56
NH_4^+	-112	1.39
NMe_4^+	-144	0.6
Mg^{2+}	-331	3.04
Ca^{2+}	-252	3.2
Sr^{2+}	-242	3.25
Ba^{2+}	-205	2.97
Zn^{2+}	-318	2.94

* All surface tension increment values are for corresponding 1 M metal chloride salts. Ionic strength difference between monovalent and divalent metal chloride should be taken into account while comparing the values.

mixed with salts. If the added salt compressed the water structure, salting out was observed. On the other hand, a marked increase of hydrophobic species solubility was seen with the salts which loosened the water structure. However, this theory involved using some arbitrary assumptions and gave significantly higher than expected salting-out constants as compared to experimentally observed values. Another popular viewpoint of explaining such salt effects is scaled particle theory.[62] This theory attributed the effects to two counteracting terms. One term was the free energy required to create a solvent cavity where solute can get solvated. Salts, in general, makes the cavity formation harder to accomplish and hence leads to salting out of hydrophobic solutes. Second term was the attractive vanderwall forces between hydrophobic solute and wall of the solvent cavity. This should lead to salting-in. The overall observed salt effect would be the sum of these two terms. This theory gave very good qualitative and quantitative correlations with the observed results and found wide acceptance even though some exceptions still needs explanation.[63] Unlike hydrocarbons, however, all proteins additionally have polar amide groups in the polymeric backbone and variable degree and chemical identity of charged amino acid residues in their side chains which are accessible to interactions with ions in salt solutions.

Even though the thermodynamic response of PNIPAM and ELPs is also driven by hydrophobic collapse and aggregation of non-polar side chains, specific ionic associations with amide group, hydrophobic groups and their effect on interfacial water structure should also be taken into account.[15,18,25,64] Infact, ions interact very specifically

to the amide groups and nonpolar groups of uncharged proteins and the overall observed effect could be just the summation of these two forces.[25,65-67]

In our results, cation effects on both ELP and PNIPAM showed some interesting qualitative similarities (Figs. 2.2, 2.3, 2.5 and 2.6). Among the monovalent ions, chlorides of smaller ions (Na^+ or K^+) salted out more as compared to larger ions (Rb^+ or Cs^+). Lithium, however, was the sole exception to this trend as it salted out lesser than even Rb and Cs ions. Larger ions, being more hydrophobic and more polarizible, will have comparatively stronger dispersion interactions with hydrophobic isopropyl moiety of PNIPAM and non-polar valine residues of V_5-120 ELP.[11,26,68] Such interaction should lead to salting-in and counteract the dominating salting-out force of chloride species. Ammonium ion also decreased the LCT to a lesser extent because of the hydrogen bonding potential of its hydrogens to the amide group. Additionally, relative to other monovalent alkali ions, it is excluded from air-water interfaces to a lesser extent.[58] These factors will partially neutralize the salting out tendency of chloride ion. Alkylated ammonium ion, on the other hand, partitions even more favorably to the polymer hydrophobic moieties making it a stronger chaotrope.[63,69] Clearly, tetramethyl ammonium chloride ion had the least effect on biopolymers phase transition temperature value.

Lithium and other divalent ions with very high charge densities are heavily hydrated and the positive charge is diffused over the associated hydration shell. These cation hydrates are speculated to interact directly to the amide group of polypeptide through their solvation shell (Fig. 2.8).[65] Such an interaction would lead to increased solubilization of polypeptide/polymer chain and would counteract the usual LCST decrease caused by chloride anion. This was clearly seen in the observed trends as all the divalent ions and lithium ion decreased the LCST to a lesser extent as compared to other alkali monovalent ions of same ionic strength. As expected, among divalent ions, magnesium was found to have the least effect on PNIPAM solubility. On the other hand, least hydrated alkaline earth metal, Ba^{2+}, had the highest impact on the LCST of both PNIPAM and ELP. At high concentrations (> 0.6 M) of all these ions, slight deviation of phase transition behavior from typical linear decrease was observed which also hints at the possible involvement of such indirect weak binding interactions with carbonyl group of amide moiety.

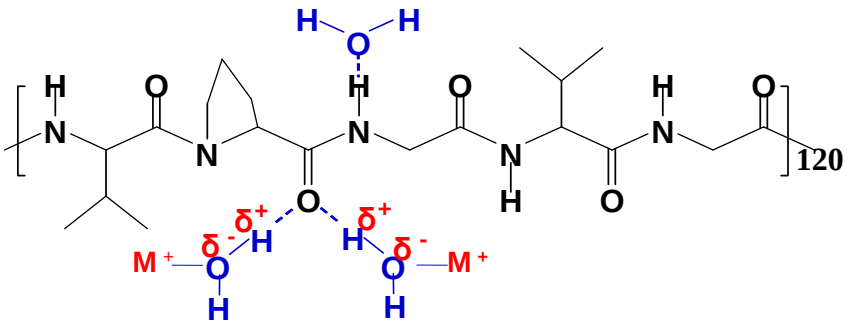

a)

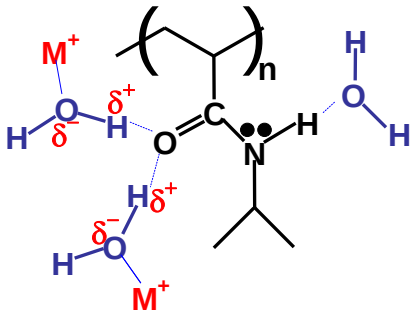

b)

Figure 2.8. a) Increased solubility of polypeptide chain through hydrogen bonding interaction of the amide with hydrated cation, $M^+(H_2O)_n$. b) Corresponding figure for PNIPAM.

This model can answer some well-known but not clearly understood questions about cations effects. For example, it can explain why cations show opposite behavior compared to anions that strongly hydrated anions usually salt out of proteins while strongly hydrated cations salt proteins into solution. Also, it solved the mystery of why anions show more pronounced effects than cations in the most of existing systems.

Quantitative analysis of the observed trends was also performed. Normalized *c* values were plotted against known hydration entropy values of different cations (Table 2.2).[57] The two parameters showed a clear inverse relationship to each other (Figs. 2.9 and 2.10). More hydrated ions including divalent ions have lower salting out constants than the less hydrated ions. A fairly good correlation of thermodynamic data of both PNIPAM and V_5-120 polypeptide with the corresponding hydration entropy values indicates a consensus mechanism of the interaction of cations with proteins/polymers. *c* values were also tested against other well known physical parameters of ions such as partial molar ionic volumes, viscosity coefficients, enthalpy of hydrations and free energy of hydrations; however the data doesn't seem to show great correlation (data not shown here).

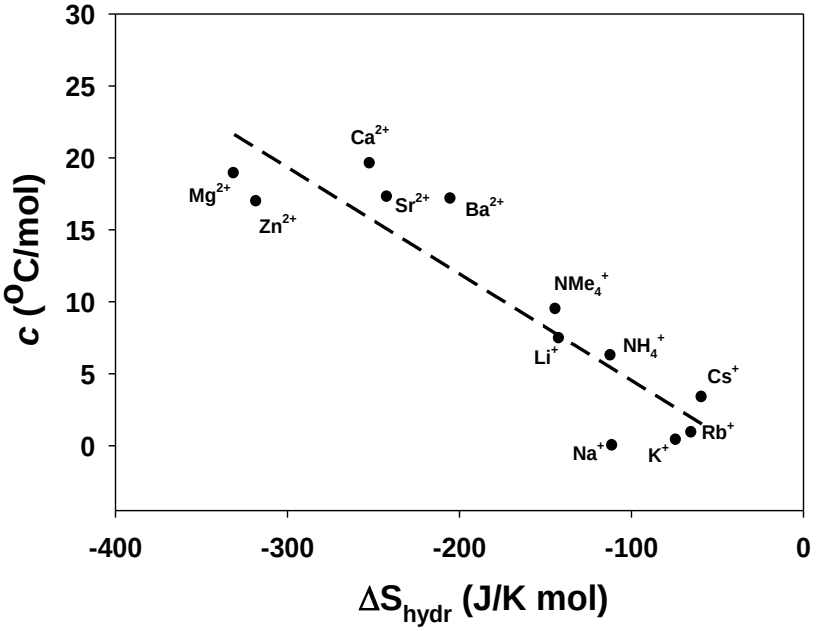

Figure 2.9. Plot of hydration entropy of the cations vs. normalized *c* values for V_5-120 ELP. The dashed black line shows the inverse correlation of the two parameters.

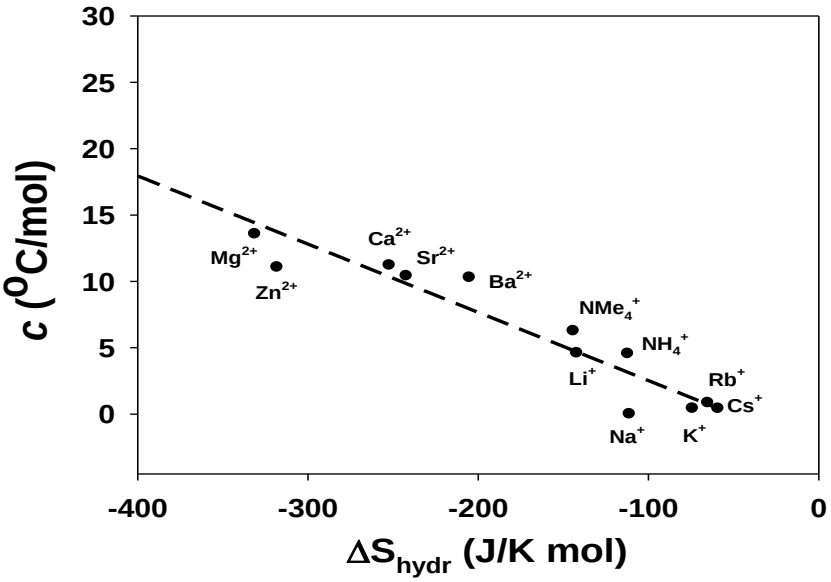

Figure 2.10. Plot of hydration entropy of the cations vs. normalized *c* values for PNIPAM. The dashed black line shows the inverse correlation of the two parameters.

Conclusions

The specific cation effects of various metal chloride salts were investigated with two model hydrophobic, neutral biomacromolecules shedding light onto the underlying molecular mechanism of such interactions. The hydrophobic collapse/aggregation process for neutral biopolymers was dominated by the anionic chloride part. However, some subtle cation interaction preferences were also observed. Large alkali cations, Rb^+ and Cs^+, and hydrophobic alkylated ammonium ions presumably solvates the hydrophobic pockets on biopolymers. Such dispersion forces leads to lesser salting-out constants for these ions. Smaller alkali cations, Na^+ and K^+, on the other hand, are mostly depleted from biopolymer surface resulting into higher salting-out constants. Phase transition process for these salt solutions is completely dominated by chloride species and its increasing surface tension effect as a function of concentration. Highly hydrated cations like lithium and divalent ions modulate the phase transition temperatures via their interaction to the amide moieties through their tightly held water hydration shell. This weak indirect interaction with amide moiety also leads to solubilization of biopolymer chains and lesser decrease in LCST values.

CHAPTER III

HOFMEISTER CATION SERIES: ROLE OF PROTEIN SURFACE CHARGE IN DETERMINING CATION SPECIFICITY

Introduction

Thermodynamic and surface-specific spectroscopic investigations were carried out on a model peptide system to explore the importance of charged groups and ion-pairing affinities in determining the overall partitioning of cations to protein surfaces and related Hofmeister effects. More specifically, a thermoresponsive elastin-like polypeptide (ELP) DV_2F-64 containing 16 aspartic acid residues was tested with a series of monovalent and divalent metal chloride salts to understand the role of such acidic residues in inducing cation specificity under physiologically relevant conditions.

For systems containing sites of negative charge, the influence of cations can be much greater. In fact, ion-pairing between mobile cations in solution and fixed titratable acetate groups on biomacromolecules is thought to affect protein-protein associations, protein folding/stability as well as macromolecular aggregation and precipitation.[19,24,70] The exact nature of these interactions should be ion specific as well as depend on the nature and charge distribution along the protein chain. Some clues about the nature and mechanisms of these interactions can be gleaned from the analogous problem of the interactions of ions with synthetic polyelectrolytes.[71-76] Nevertheless, the ion specific nature of the interactions between sites of negative charge on proteins and cations still remains poorly understood.

The nature of cation interactions with sites of negative charge on proteins is inherently interfacial. Indeed, such interactions take place at the protein/water interface. As such, surface specific techniques such as vibrational sum frequency spectroscopy (VSFS) can potentially provide very useful vibrational information about these interactions.[43,50-51] Herein, we used results from VSFS experiments along with complementary thermodynamic data to help elucidate the nature of cation-acetate interactions. To do this, we employed specifically designed elastin-like polypeptide (ELPs), for our experiments (Chapter I). The relative hydrophobicity/hydrophilicity of ELPs can be easily tuned by inserting specific amino acid residues at the guest residue location in the constituent pentapeptide units.

In this particular study, we wished to employ a polypeptide containing aspartic acid residues at one quarter of the guest resides sites. The other three-quarters of the sites contained the hydrophobic valine and phenylalanine residues. The total chain length of the ELP was 320 amino acids or 64 pentapeptide repeats. It is designated ELP DV_2F-64, which refers to the fact that aspartic acid, valine and phenylalanine residues are present in the guest residue sites in a 1:2:1 ratio. Since there are 64 pentapeptides, the molecule possesses 16 aspartic acid residues, which imparts a significant negative charge at neutral and basic pH values. The results indicated that the partitioning of cations to the ELP/water interface could be directly correlated with the cations effects on the LCST of the polypeptide. The results followed a direct Hofmeister series.

Experimental

LiCl, NaCl, KCl, RbCl, CsCl, NH_4Cl, NMe_4Cl, $MgCl_2$, $CaCl_2$, $SrCl_2$, $BaCl_2$, $ZnCl_2$, Tris (hydroxymethyl)-aminomethane and Tris (hydroxymethyl) aminomethane hydrochloride buffers were purchased from Sigma Aldrich (> 99% Purity). All salt solutions and buffers were prepared by dissolving the dry salts in freshly purified deionized water obtained from a NANOpure Ultrapure Water System (Barnstead, Dubuque, IA) having a minimum resistivity of 18.1 MΩ.cm. For VSFS experiments in heavy water, salt solutions were prepared in 99.9% isotopically pure D_2O, which was obtained from Cambridge Isotope Laboratories, Inc. (Andover, MA).

Additionally, it should be noted that the zinc salts can form zinc hydroxide in alkaline solutions.[77-78] However, under the current experimental conditions, at pH 9.76, the concentration of hydroxide ions is fairly low (~ 5.75×10^{-5} M). The observation of very strong binding of zinc to polypeptide at low millimolar salt concentrations is most definitely from the very favorable Zn^{2+}-acetate binding interactions rather than due to the formation and adsorption of $(ZnOH)^+$. Also, no significant drop in pH of buffered solution was seen on dissolving zinc chloride salt.

ELP Preparation

The pET plasmids having an inserted gene sequence for DV_2F-64 ELP were constructed using the recursive directional ligation method.[29] This was followed by the transformation of the plasmids into BLR (DE3) competent *E. coli* cells (Novagen®, MERCK Chemicals). The cells were expressed for 24 hrs at 37 ^oC in TB Dry® cell culture growth medium (MO Bio Laboratories, Inc.). Expression was done in ampicillin

containing medium so as to prevent the growth of undesired bacteria. Cells were then lysed via sonication and the cell debris was removed using centrifugation. Treatment of the resulting supernatant with poly(ethyleneimine) led to the removal of unwanted nucleic acids. pH control during this step is very critical since this positively charged polymer may also precipitate out negatively charged ELP along with nucleic acids. The ELPs reversible thermoresponsive nature and sensitivity towards inorganic salts was utilized for its isolation and purification. Specifically, ELP containing solutions were subjected to a series of inverse transition cycles (ITC). In short, 1 M NaCl was added to an ELP solution followed by incubation at 50 ^{o}C for 1 hr. White precipitates of ELP were collected as a pellet via centrifugation and this pellet was then redissolved in cold sodium phosphate buffer (10mM, pH 7). Generally, 2-3 rounds of the ITC cycles were sufficient to remove all unwanted impurities. Sodium dodecyl sulfate-polyacrylamide gel electrophoresis (SDS-PAGE) was performed to confirm the purity and molecular weight of the final product. The concentration of ELP molecules in aqueous solution was determined by UV absorbance measurements at 280 nm (ε = 5690 $M^{-1}cm^{-1}$).[29] A prominent absorption peak was also observed at ~ 258 nm. This corresponds to the absorption from multiple phenylalanine residues. Dialysis of the final purified polypeptide solution was done against purified deionized water to remove any residual salts. Finally, the polypeptide samples were lyophilized and stored at -80 ^{o}C until their usage in thermodynamic and spectroscopic measurements.

LCST measurements

1 M Stock solutions of all of the monovalent and divalent chloride salts were prepared in 10 mM Tris (hydroxymethyl)-aminomethane buffer at pH 9.76. Salt solutions of the desired concentration were obtained by diluting the stock solutions with pure buffer. For all thermodynamic measurements, lyophilized solid samples of DV_2F-64 ELP were dissolved in salt solutions to obtain a final peptide concentration of 10 mg/ml. Prior to taking phase transition measurements, all peptide solutions were kept in an ice bath for ~30 minutes to ensure complete solubilization. The phase transition temperature measurements were made with an automated melting point apparatus (Optimelt^{TM} MPA 100, Stanford Research Systems). In a typical LCST measurement, three capillary tubes filled with identical ELP solutions were placed in the heating chamber of the melting point device. The samples were then subjected to a gradual temperature ramp and the light scattering intensity of the samples was recorded as a function of temperature. A ramp rate of 0.5 ^{o}C/ min was used for all measurements. The in-built camera on the instrument captured real-time images of the samples and then used digital image processing to determine the onset of the LCST (Chapter I). All LCST values reported in this study are an average of six measurements. The data obtained was highly reproducible and used just ~10 μL ELP sample per capillary tube.

VSFS measurements

In VSFS experiment, a visible beam and an IR beam are temporally and spatially overlapped at the sample surface to generate a sum-frequency response. An enhancement in sum frequency beam signal is observed when the incoming IR beam is

in resonance with the any vibrationally active species at the surface. VSFS spectra were taken with a standard VSFS setup as described in detail elsewhere (Chapter I).[50-51] Briefly, a passive-active mode locked Nd:YAG laser (PY61C, Continuum, Santa Clara, CA) equipped with a negative feedback loop in the oscillator cavity was used to generate a fundamental 1064 laser beam of 50 mJ/pulse energy with a 17 ps pulse duration. The laser pulse was pulsed at 20 Hz. The 1064 nm beam was then sent through an optical parametric generation/amplification (OPG/OPA) stage (LaserVision, Bellevue, WA) which resulted in the generation of a frequency-doubled visible beam (532 nm) and a tunable mid-infrared beam. The frequency of the IR beam could be tuned from 2000-4000 cm^{-1}. The visible and infrared beams were then spatially and temporally aligned at an air/water interface in a Langmuir trough and the resulting VSFS signal beam was collected using a photomultiplier tube (Hamamatsu, Japan). In this particular study, the IR beam was continuously tuned between 2750 cm^{-1} to 3800 cm^{-1} with a typical power of ~ 0.6 mJ/pulse at the sample stage. The power of incoming 532 nm beam was 1 mJ/pulse.

To take a VSFS measurement, 35 ml of salt solutions were placed in the Langmuir trough (Model 601M, Nima, U.K.). Next, a 40 μL droplet of a 10 mg/ml stock solution of DV_2F-64 ELP was added to the top of the salt solution in the trough. This concentration of polypeptide was sufficient to rapidly form a highly reproducible saturated Gibbs monolayer at the air-water interface (Fig. 3.1a). Infact, control experiments demonstrated that increasing the concentration of the added polypeptide solution did not affect the VSFS spectrum. The presence of multiple aspartic acid

residues generates an electric field which aligns the interfacial water molecules (Fig. 3.1b). An equilibration time of 10 minute was given for the monolayer to be stabilized before starting any VSFS experiments. Longer waiting times were also found to have negligible impact on the obtained spectrum profile and intensities. All the spectra were collected with the ssp (s-sum frequency beam, s-visible beam, p-infrared beam) polarization combination.

The VSFS spectra taken in this study were all collected over a time period of 40 minutes. The first peak located near 3200 cm^{-1} has been assigned to the OH symmetric stretch of more tetrahedrally coordinated water molecules. The second peak centered around 3400 cm^{-1} is generally attributed to waters with more disordered hydrogen bonding.[41] The intensity of the SFG signal, I_{SFG} is proportional to the intensities of the input visible, I_{vis}, and infrared, $I_{IR,}$ laser beams as shown:

$$I_{SFG} \propto \left| \chi_{eff}^{(2)} \right|^2 \bullet I_{vis} \bullet I_{IR} \tag{3.1}$$

where $\chi_{eff}^{(2)}$ is the effective second order non-linear susceptibility which can be further expressed as:

$$\chi_{eff}^{(2)} = \chi_{NR}^{(2)} + \chi_{R}^{(2)} = \chi_{NR}^{(2)} + \sum_{q} \frac{A_q}{\omega_{IR} - \omega_q + i\Gamma_q} \tag{3.2}$$

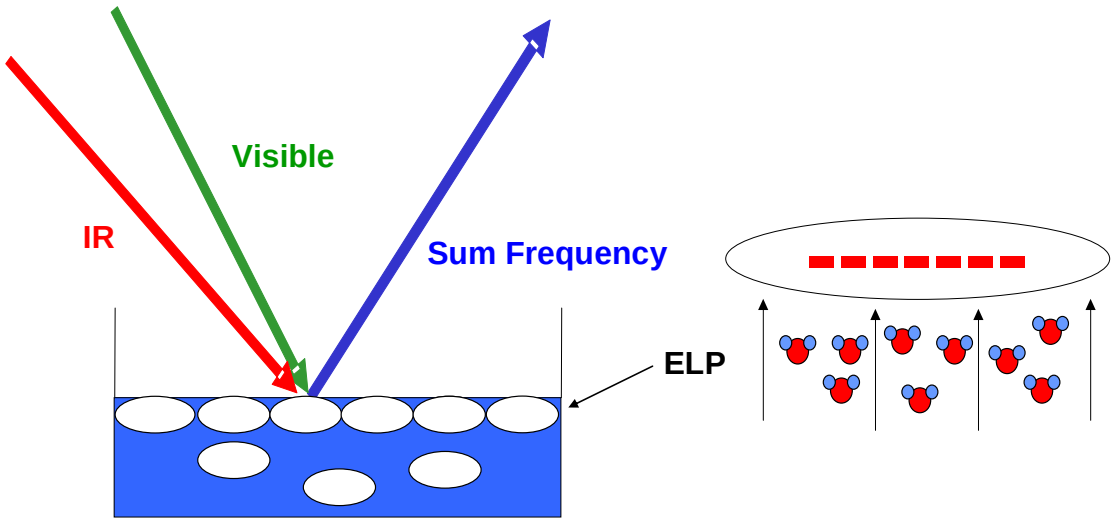

Figure 3.1. a) Schematic diagram showing the formation of Gibbs monolayer of ELP at the air-water interface. b) Alignment of water molecules close to the negative charged peptide interface. The pictures are only representative of the overall phenomena and are not drawn to scale.

Here, $\chi_{NR}^{(2)}$ is the frequency-independent nonresonant term and $\chi_{R}^{(2)}$ is frequency-dependent resonant term. Furthermore, $\chi_{R}^{(2)}$ of *q*th resonant mode can be simplified as a function of the oscillator strength, A_q, the resonant frequency, ω_q, the peak width, Γ_q, and the frequency of input infrared laser, ω_{IR}.

Results

Firstly, the LCST values of DV_2F-64 ELP were recorded as a function of solution pH (Fig. 3.2.) At low pH, aspartic acid residues of ELP were in fully protonated form. The hydrophobic collapse of ELP was very easier under such conditions, a result which was clearly visible in lower LCST values at low pH values. As the pH of solution was increased, more and more aspartic acid residues got deprotonated. The electrostatic repulsion between negatively charged aspartic acid residues lead to a dramatic increase in the LCST values of ELP. Infact, a very sharp increase in the LCST response was seen close to pH 6.5 which is presumably the isoelctric point of this polypeptide. Once all of the aspartic acid residues were fully deprotonated, as expected, no further significant increase in LCST values were seen. pH 9.76 was chosen for running further experiments so as to investigate specific interactions between negatively charged aspartate groups and wide variety of biologically relevant cations.

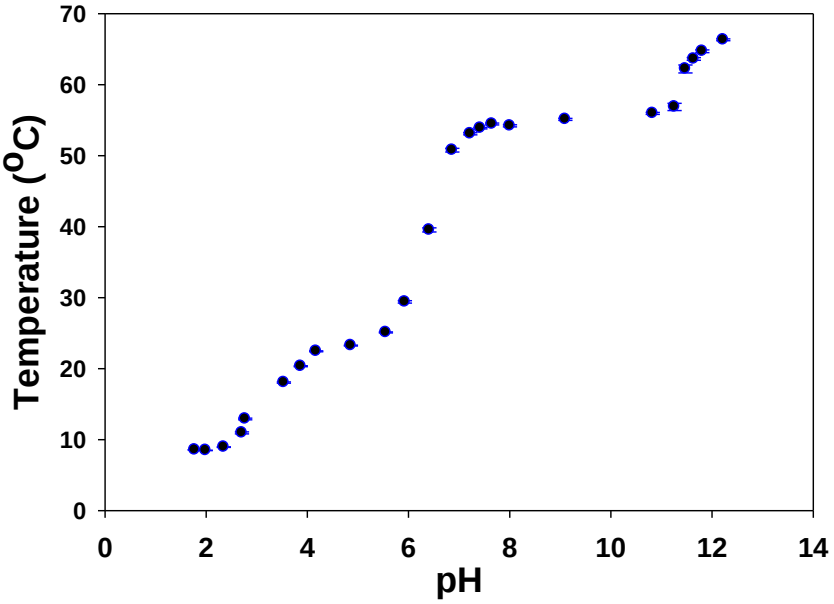

Figure 3.2. LCST values of ELP DV_2F-64 as a function of changing pH of solution. All measurements were done with 10 mg/ml ELP dissolved in 300 mM sodium chloride solutions in 10 mM sodium phosphate buffer of respective pH. Each data point represents an average of six measurements.

LCST data of ELP DV_2F-64 with chloride salts

Phase transition temperatures of 10 mg/ml aqueous solutions of ELP DV_2F-64 at pH 9.76 were measured as a function of salt type and concentration for 12 different chloride salts. Under these solution conditions, the acidic polypeptide residues were almost completely deprotonated (Fig. 3.2). This pH and peptide concentration were chosen to allow us to carry out thermodynamic measurements over a wide range of temperature and salt concentrations. Fig. 3.3. shows the effect of divalent chloride salts on the LCST value of the ELP for divalent metal cations in a range from 0 to 1 M salt. The addition of these salts to the polypeptide solution imparted a dramatic exponential decrease in the phase transition temperature in the lower concentration regime (< 100 mM salt). A shallower and more linear decrease was found as the salt concentration was further increased. At low salt concentrations (<100 mM), the order of decreasing the LCST was:

$$Zn^{2+} > Ca^{2+} > Ba^{2+} > Sr^{2+} > Mg^{2+}$$

In other words, Zn^{2+} depressed the LCST the most in this regime, while Mg^{2+} lowered this value the least. The order rearranges at higher salt concentrations to $Zn^{2+} > Ba^{2+} > Sr^{2+} > Ca^{2+} > Mg^{2+}$. In other words, the relative position of Ca^{2+} changes substantially.

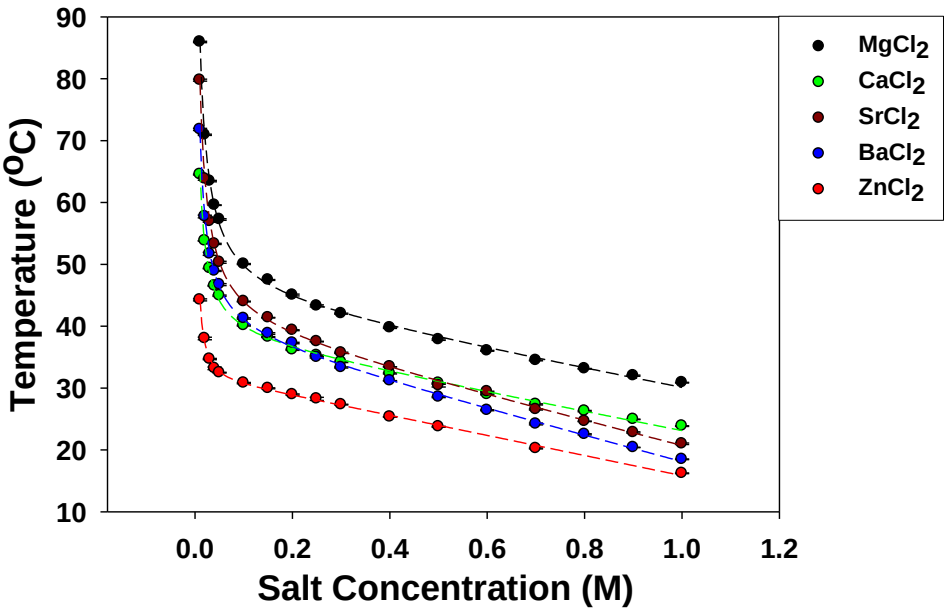

Figure 3.3. LCST response of ELP DV_2F-64 as a function of varying concentration and identity of divalent metal chlorides at high pH. All experiments were performed with 10 mg/ml ELP concentration in 10 mM tris buffer at pH 9.76. Each data point represents an average of six measurements and the dashed lines are the best fits to the data points.

Fig. 3.4. shows the analogous thermodynamic data for ELP DV_2F-64 in the presence of increasing concentrations of monovalent chloride salts. The overall trends are similar with the divalent cations. However, the initial exponential decrease in the LCST takes place up to 500 mM salt. Infact, atleast 250 mM monovalent salt concentration was required to observe the LCST of ELP within experimental range limitation. This observation is very striking especially when compared with the LCST values of divalent ions where only 10 mM divalent ion salt concentration was required to collect the first data point (Fig. 3.3). The ordering of the initial decrease was:

$$NH_4^+ > Li^+ > Na^+ > K^+ > Rb^+ \geq Cs^+ > NMe_4^+$$

Again, there is considerable switching of the order at higher salt concentrations. At 1 M concentrations, salting out efficiency was found to be: $Na^+ \sim K^+ > Rb^+ > NH_4^+ > Cs^+ > Li^+ > NMe_4^+$.

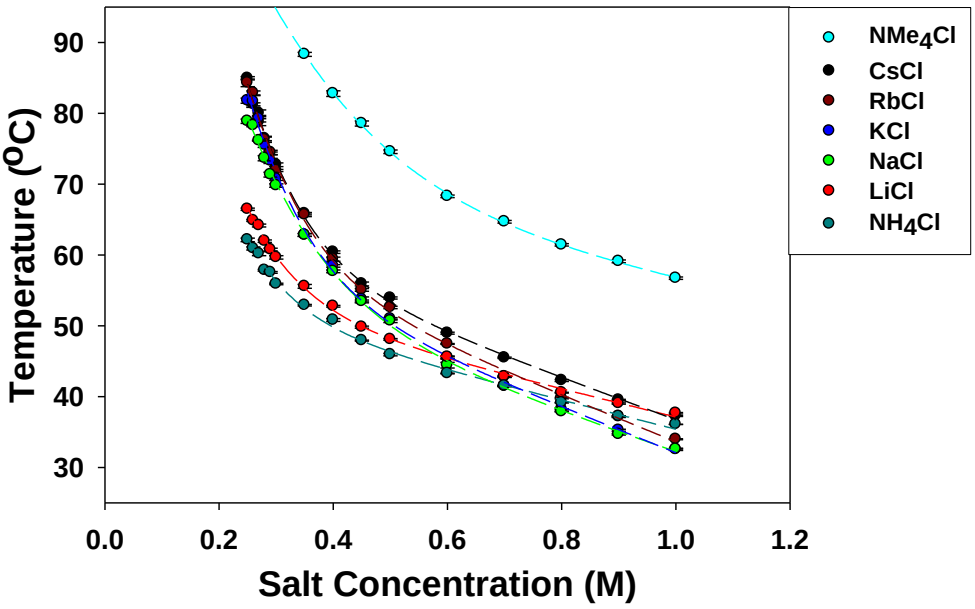

Figure 3.4. LCST response of ELP DV_2F-64 as a function of varying concentration and identity of monovalent metal chlorides at high pH. All experiments were performed with 10 mg/ml ELP concentration in 10 mM tris buffer at pH 9.76. Each data point represents an average of six measurements and the dashed lines are the best fits to the data points.

Fitting of thermodynamic data

The thermodynamic behavior of polypeptide in the presence of salts can be rationalized in terms of specific interactions of the cations with the charged, polar and hydrophobic regions of the peptide as well as modulation of the interfacial water structure. At high pH, multiple aspartic acids on the peptide surface exist in their deprotonated form. This imparts a very high negative charge to the ELP. As a result, the initial LCST of the ELP is quite high because of electrostatic repulsions between the negative charge aspartic acid residues (Fig. 3.2). It should be noted that, in the absence of any salt, the ELP phase transition process could not be observed till 105 ^{o}C (data not shown). Addition of salts results in a strong partitioning of the positively charged cations to the ELP surface. This neutralizes the negative charge, which allows the inverse phase transition to take place at lower temperature. Such ion pairing between the acetate moieties and the cations should be correlated to the exponential decrease in the ELP collapse temperature at low salt concentrations (Figs. 3.3 and 3.4).[79] Once this relatively strong ion pairing interaction has been saturated, the significantly weaker interactions of the ions with the peptide backbone and hydrophobic residues become the dominant factor in modulating the LCST.

These two types of interactions governing the LCST can be modeled using eqn. 3.3, which consists of a constant, a modified Langmuir binding isotherm and a linear term.[79]

$$T = T_0 + c[M] + \frac{B_{\max}[M]e^{-b[M]}}{K_d + [M]e^{-b[M]}} \qquad (3.3)$$

where T_0 is the phase transition temperature of ELP in the absence of any salt; [*M*] is the molar salt concentration. The constant, B_{max}, has units of temperature and denotes the maximum decrease in the LCST when all of the acetate moieties on the ELP are paired with cations. The constant, *b*, has units of inverse molarity and is related to the strength of the electrostatic interactions between the negatively charged polypeptide and the cations. The constant, K_d, represents the apparent binding constant for the specific interactions of the cations to the putative acetate binding sites. The lower the value of K_d, the stronger the binding affinity should be. The constant, *c*, has units of temperature/molarity and represents the linear change in the interfacial tension of the polypeptide/water interface as salt is added to the solution. The dashed lines in Fig. 3.3. and Fig. 3.4. are the fits of the experimental data to eqn. 3.3. As can be seen clearly, the fits appear to be extremely good. From the fitting, for all monovalent and divalent salts, extrapolated T_0 seems to be close to 140 ^{o}C. The abstracted values of K_d, B_{max}, b, c obtained from fits are summarized in Table 3.1.

Table 3.1. Fitted values of different parameters obtained by plotting high pH LCST data of ELP DV_2F-64 with 12 different chloride salt solutions using equation 3.3.

Cation	B_{max} **(^oC)**	K_d **(M)**	b **(M^{-1})**	c **(^oC/mol)**
Mg^{2+}	-95.5	0.0079	-0.003	-15.0
Ca^{2+}	-102.0	0.0037	-0.106	-15.1
Sr^{2+}	-100.1	0.0066	-0.001	-19.6
Ba^{2+}	-101.4	0.0049	-0.002	-20.8
Zn^{2+}	-107.8	0.0016	-17.2	-16.2
Li^{+}	-84.9	0.28	-6.35	-17.7
Na^{+}	-80.4	0.57	-6.03	-27.4
K^{+}	-75.6	1.21	-8.75	-32.1
Rb^{+}	-73.5	1.30	-9.05	-32.8
Cs^{+}	-73.5	1.35	-9.36	-29.6
NH_4^{+}	-87.2	0.18	-5.53	-16.9
NMe_4^{+}	-58.0	2.0	-7.66	-25.3

The apparent ion pairing contribution to the overall partitioning of the cations to the ELP surface can be easily visualized by replotting the binding curve and linear portion of the fits to the data separately.[15,79] Subtracting ($T_0 + c[M]$) from the phase transition temperature data in Figs. 3.3 and 3.4 yields binding curves for the divalent and monovalent cations to the negatively charged ELPs as shown in Fig. 3.5a and Fig. 3.5b, respectively. As can be seen, the apparent binding constants of the cations to the ELP surface show saturation behavior by ~100 mM for the divalent cations and ~500 mM for the monovalent cations. Moreover, the B_{max} values for the divalent cations are clustered around 100 $^{\circ}$C, whereas the monovalent numbers are closer to 80 $^{\circ}$C with the exception of NMe_4^+, which is somewhat lower.

Fig. 3.6. displays the residual linear decrease in the LCST values for both the divalent and monovalent ions as a function of increasing salt concentration. The linear salting out effect should be dominated by the chloride anions rather than the monovalent or divalent cations (Chapter II).[4,6] Indeed, the difference in *c* values between Rb^+ and Mg^{2+} is only about a factor of two. This stands in stark contrast to the differences in K_d and *b* values for the various cations which is as large as three orders of magnitude. This is in agreement with the notion that specific cation effects are profound for ion pairing, but only relatively modest for surface tension. It should be noted that modulating the anions from very chaotropic to very kosmotropic can change the surface tension by about a factor of five.[4,15,56,58]

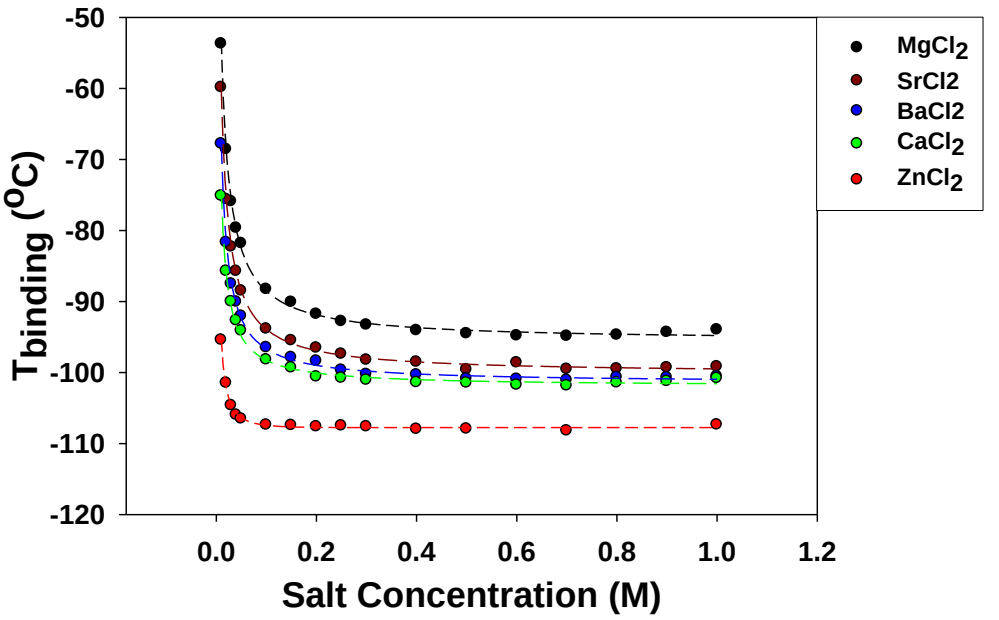

(a)

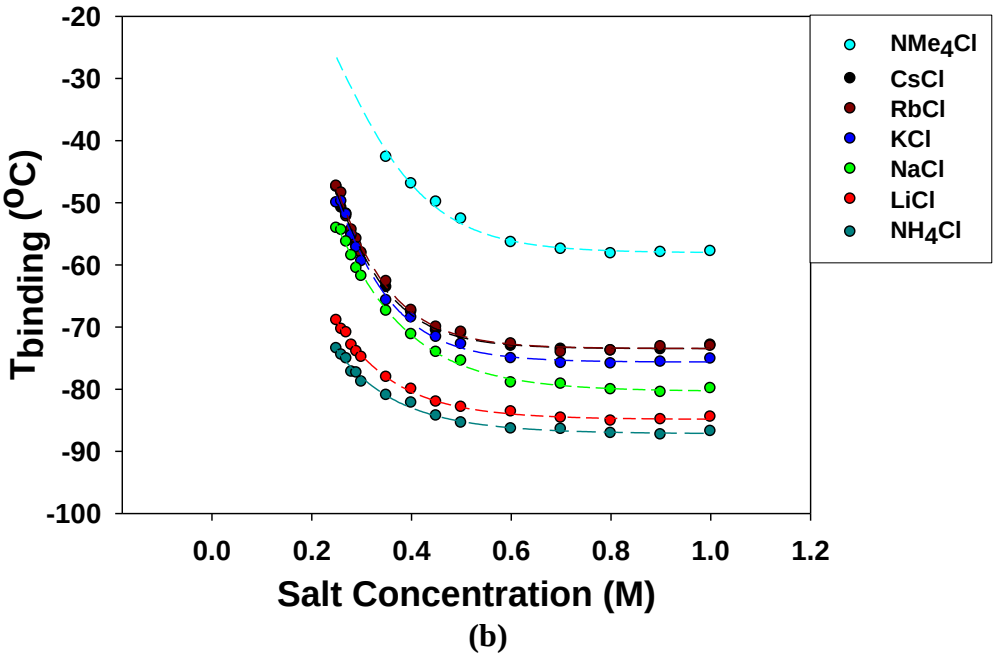

(b)

Figure 3.5. (a) Residual cloud-point temperature data for divalent metal chloride salts obtained from Fig. 3.3 after subtracting the linear portion from the phase transition curves. (b) Corresponding data for monovalent chloride salts after subtracting linear portion from Fig. 3.4. The dashed lines represent best fits to the data points.

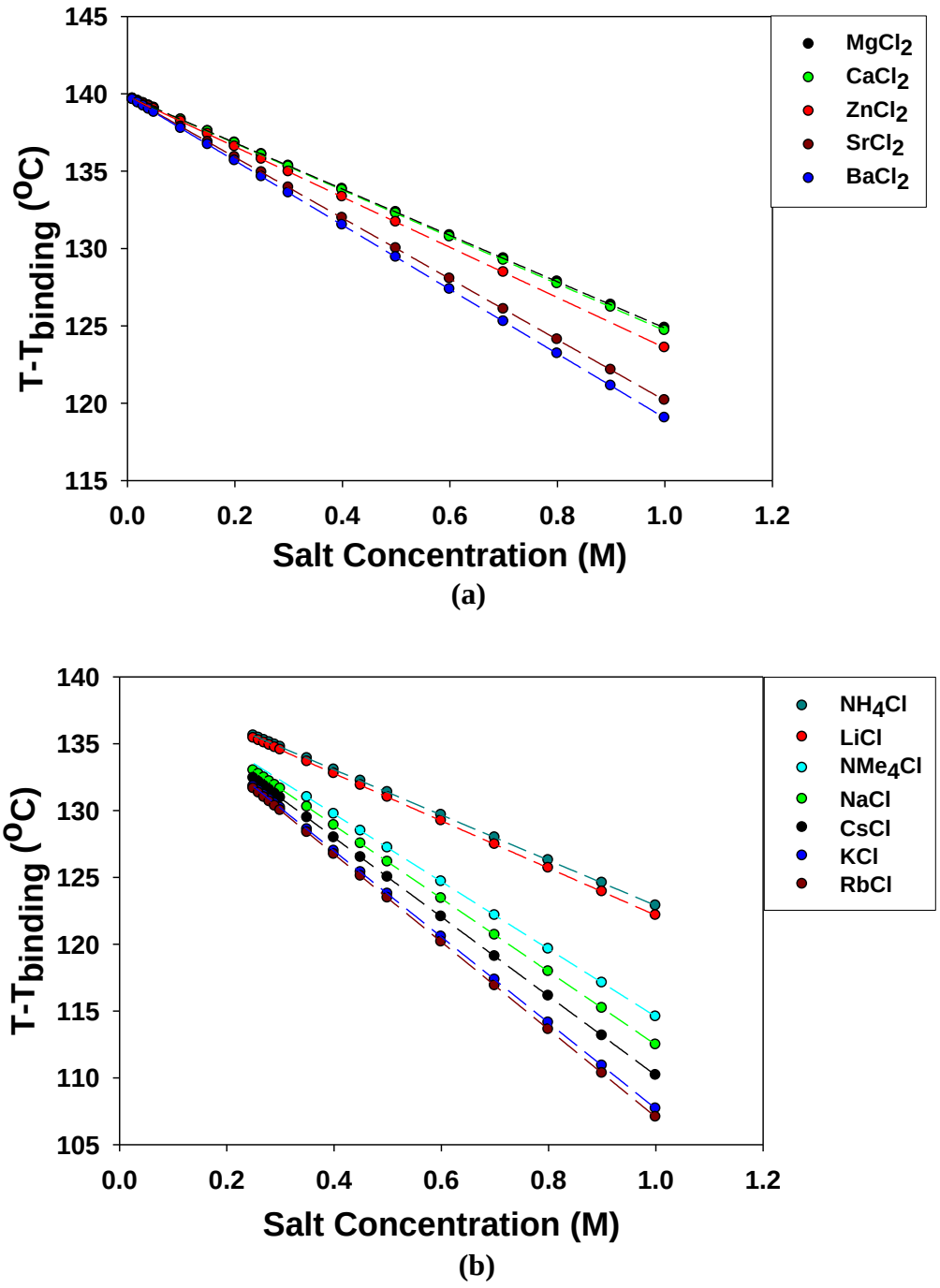

Figure 3.6. (a) Residual cloud-point temperature data for divalent metal chloride salts obtained from Fig. 3.3 after subtracting the binding portion from the phase transition curves. (b) Corresponding data for monovalent chloride salts after subtracting the binding part from Fig. 3.4. The dashed lines represent best fits to the data points.

LCST measurements at low pH

As a control experiment, ELP LCST was also measured at pH 2.5 in the presence of all the monovalent and divalent metal chloride salts (Fig. 3.7). Aspartate residues were mostly protonated under such conditions. A very minimal linear decease in the LCST values was observed and the differences between different cations were barely discernible at low concentrations. Interestingly, exponential binding part was missing at low pH measurements. At Low pH, the salt interactions with this protonated, mostly hydrophobic ELP are primarily dominated by the dispersion forces and surface tension effects of chloride anion (Chapter II). This further highlights the importance of negatively charged acetate groups in inducing specificity among cations under physiological conditions.

VSFS spectral features of ELP DV_2F-64

To obtain a deeper molecular level understanding of cation-ELP interactions, surface specific spectroscopic measurements were performed. VSFS measurements of a Gibbs monolayer of ELP DV_2F-64 were recorded at various salt concentrations and pH conditions. In a first set of experiments, VSFS spectra of an ELP DV_2F-64 monolayer were taken at a series of different pH values (Fig. 3.8). Each spectrum had the same spectroscopic features in the CH stretch region (~ 2800-3100 cm^{-1}). The major peak near 2875 cm^{-1} arises due to the symmetric stretch of methyl groups on the valine residues. A somewhat less prominent and very weak feature shows up as a shoulder near 2840 cm^{-1}, which can be assigned to a CH_2 symmetric stretch. Another major peak was clearly visible at nearly 2950 cm^{-1} which is generally attributed to the combination of a

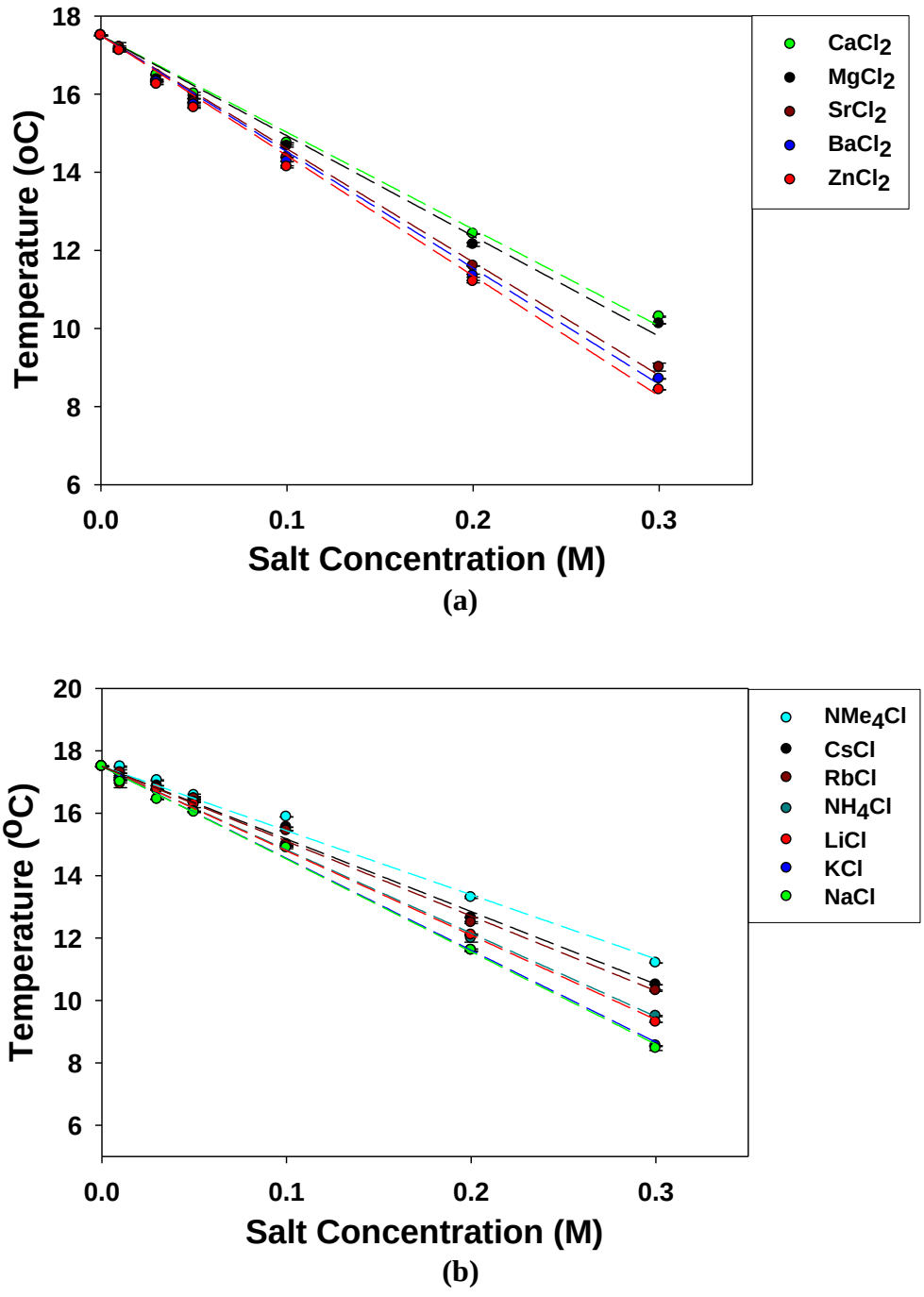

Figure 3.7. LCST response of ELP DV_2F-64 at low pH in the presence of (a) divalent chloride salts (b) monovalent chloride salts. All experiments were performed with 10 mg/ml ELP concentration in 10 mM tris HCl buffer at pH 2.5. Each data point represents an average of six measurements and the dashed lines are the best fits to the data points.

Fermi resonance and the methyl asymmetric stretch.[51] The weak band near 3050 cm^{-1} can be attributed to the aromatic CH stretch of the phenylalanine residues present in the ELP. The over all intensity from the CH region indicates a high degree of ordering of the polypeptide at air/water interface. This is expected, as hydrophobic valine and phenylalanine side chains should be oriented into the air and away from the aqueous solution. There are some apparent differences in peak heights as a function of pH, but these are caused by interference between the CH and OH stretch regions. Running control experiments in D_2O demonstrates that the CH stretch features remain largely unchanged as the pH is modulated (Fig. 3.9).

The OH stretching region contains two distinct, broad spectral features. The first peak is centered around 3200 cm^{-1} and can be assigned to the OH stretch of interfacial water molecules in a mostly tetrahedral conformation.[41,51] The second prominent OH stretching peak, centered close to 3450 cm^{-1}, is typically assigned to water molecules that lack a full complement of hydrogen bonds. The oscillator strengths in the OH region are highly sensitive to the pH of the bulk solution pH. This is expected, since more and more aspartic acid residues get deprotonated as the pH is increased. This in turn imparts a strong negatively charged potential at the peptide/water interface, which should align adjacent water molecules. Eventually, at high enough pH, nearly all the acidic residues should be completely deprotonated. This is nearly true by pH 7.29, but is certainly true by pH 9.76. These numbers are in excellent agreement with LCST data for ELP DV_2F-64, which shows a continuous rise in the inverse phase transition temperature starting around pH 2 and level off near pH 8 (Fig. 3.2).

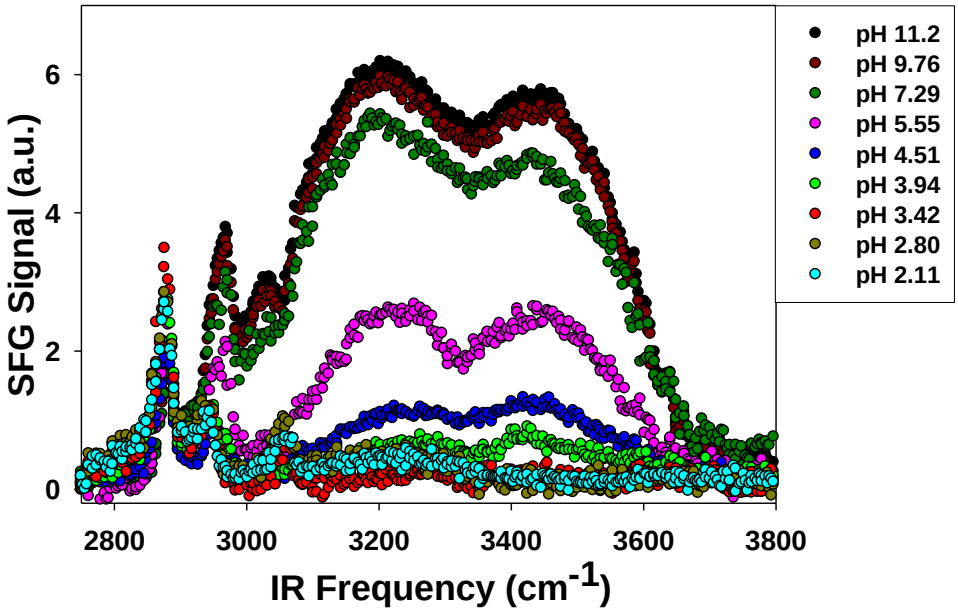

Figure 3.8. VSFS spectra of ELP DV_2F-64 as a function of solution pH. All experiments were performed with 1 mM tris buffer. pH was modulated by adding HCl/NaOH.

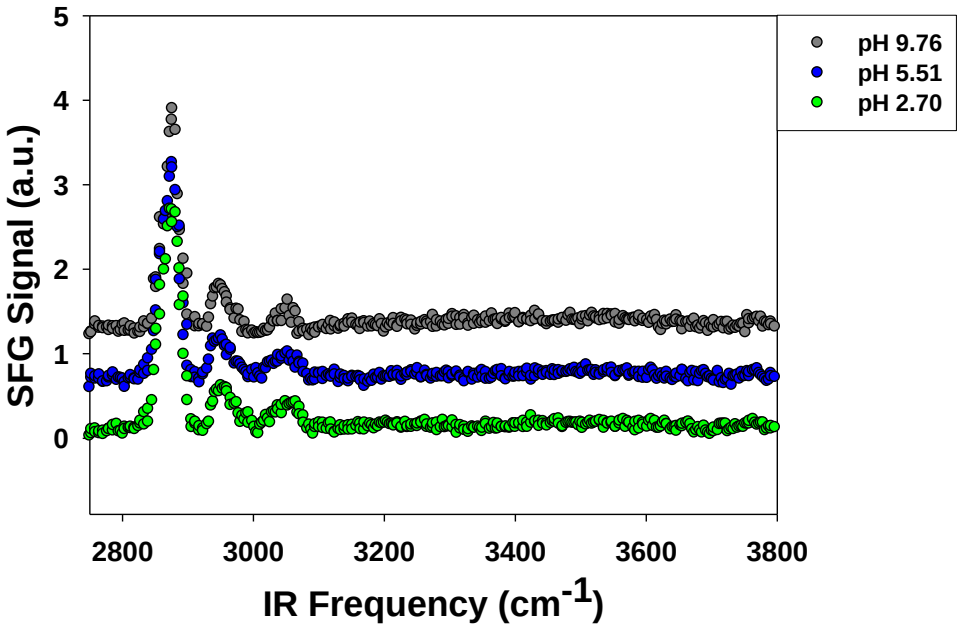

Figure 3.9. VSFS spectra of ELP DV_2F-64 as a function of pH of deuterated solutions. All experiments were performed with 1 mM tris buffer made in 99.9 % D_2O. pH was adjusted by adding Conc. HCl. The spectra are offset by 0.6 units each for the sake of clarity.

Specific binding of cations to the negatively charged ELP surface

To investigate the partitioning of divalent metal ions to the negatively charged peptide interface, VSFS spectra of ELP DV_2F-64 were taken at pH 9.76 in the presence of 16.66 mM of various divalent metal chloride salts (Fig. 3.10). As the divalent metal ions bind to the negatively charged aspartate moieties, the interfacial charge will be neutralized, leading to lower signal intensity in the OH stretch region. The relatively low salt concentration was chosen to correspond to the steep exponential decay portion of the LCST data in Fig. 3.3. As can be seen from the data in Fig. 3.10, the ion that led to the greatest attenuation in water signal intensity was Zn^{2+}, while Mg^{2+} had the smallest effect. The order of the ions was: $Zn^{2+} > Ca^{2+} > Ba^{2+} > Sr^{2+} > Mg^{2+}$. This is the identical order to that found at low salt concentrations in Fig. 3.3 and also matches the order of the K_d values for the putative acetate-divalent cation data provided in Table 3.1.

Fig. 3.11. shows the corresponding specific interactions observed with monovalent chloride ions at the same pH and also with the identical ionic strength as in Fig. 3.10. These conditions correspond to the exponential portion of the LCST data in Fig. 3.4. The overall binding order was found to be: $NH_4^+ > Li^+ \geq Na^+ \geq K^+ > Rb^+ \geq Cs^+ > NMe_4^+$. Again this is identical to the low concentration ordering found in Fig. 3.4 and the corresponding K_d values listed in Table 3.1.

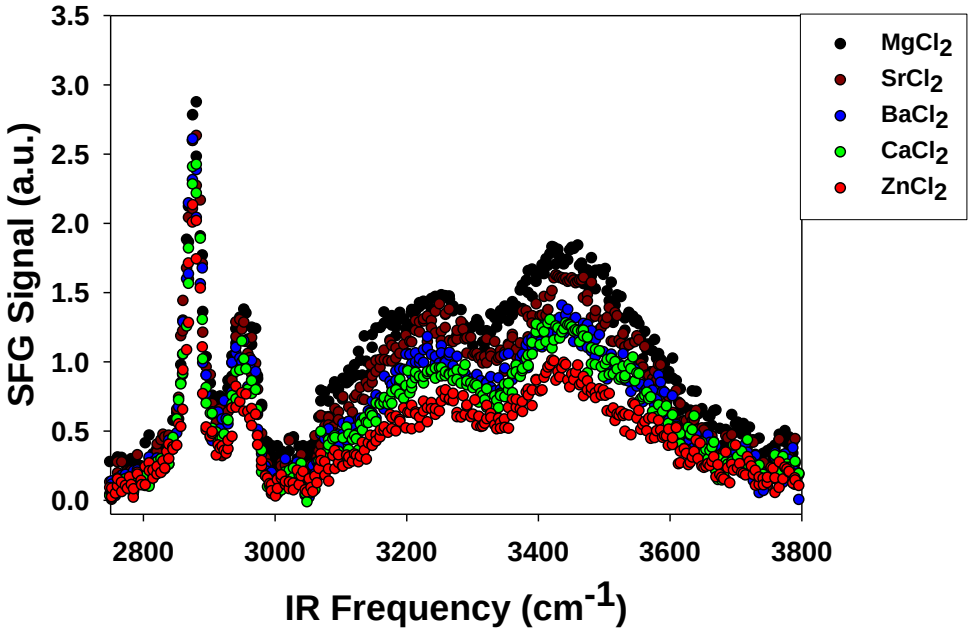

Figure 3.10. VSFS spectra of ELP DV_2F-64 in the presence of various divalent metal chloride solutions at high pH. All experiments were performed with 16.66 mM concentration of salt solutions in 1 mM Tris buffer, pH 9.76. Each spectrum represents an average of three scans.

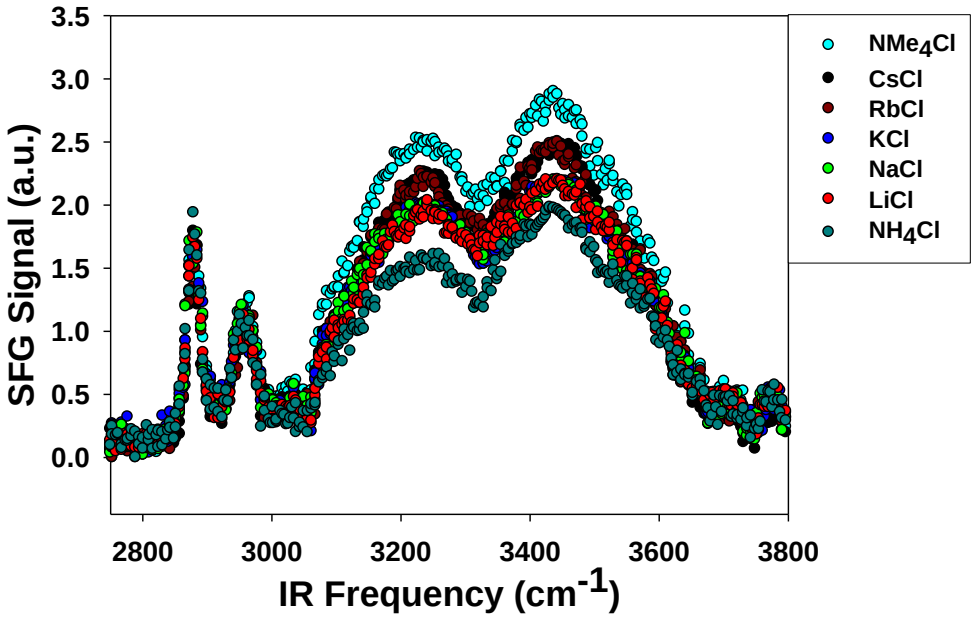

Figure 3.11. VSFS spectra of ELP DV_2F-64 in the presence of various monovalent metal chloride solutions at high pH. All experiments were performed with 50 mM concentration of salt solutions in 1 mM Tris buffer, pH 9.76. Each spectrum represents an average of three scans.

It should be noted that the VSFS spectra in both Fig. 3.10 and Fig. 3.11 also showed some very small apparent signal intensity changes even in the CH stretching region (2800-3100 cm^{-1}). These changes are a result of interference with the OH stretch region and the actual CH stretch intensities remained unchanged. As with the pH changes, this can also be demonstrated by running control experiments in D_2O (Fig. 3.12 and Fig. 3.13). When the experiments are run in D_2O, only C-H stretching features can be seen. The O-D stretching bands which occur close to 2600 cm^{-1} cannot be seen in the normal spectrum scanning range. Such control experiments demonstrate that the surface concentration and orientation of the peptides remained essentially unchanged regardless of the particular salt that was employed. Moreover, all of the intensity changes in the spectra are a result of the changes in signal intensity in the OH stretch region.[50]

VSFS spectra of protonated ELP DV_2F-64 in the presence of salts

The presence of a significant number of negatively charged residues should be overriding factor causing cation specificity in both the above VSFS and LCST data at low salt concentration. To test this, the VSFS measurements were repeated at pH 2.7 under otherwise identical conditions. Fig. 3.14 shows the VSFS response for the divalent chloride salts, while the monovalent chloride salts data is in Fig. 3.15. As can be clearly seen, all the spectra are essentially identical within experimental error. This means that the protonated aspartate residues lead to essentially no cation specific interactions in the salt concentration range employed.

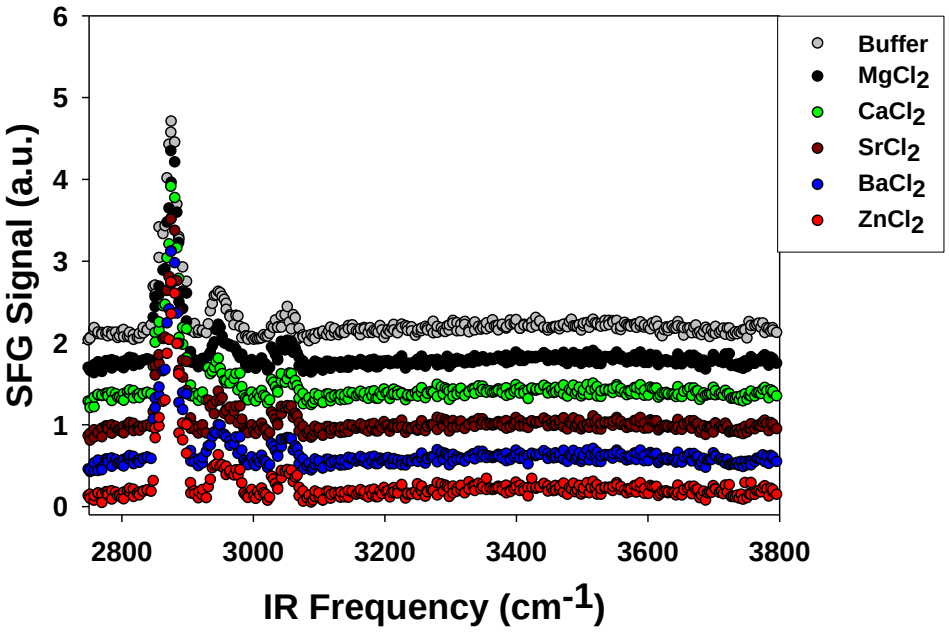

Figure 3.12. VSFS spectra of ELP DV_2F-64 in the presence of deuterated solutions of 16.66 mM divalent metal chloride salts at high pH. All experiments were performed with 1 mM tris buffer made in 99.9 % D_2O (pH 9.76). The spectra are offset by 0.4 units each for the sake of clarity.

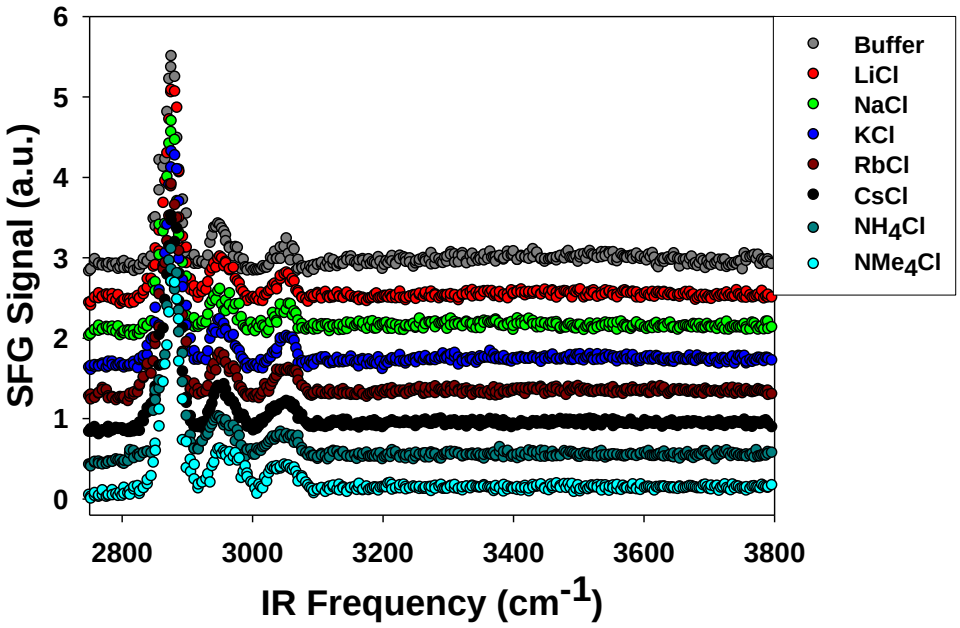

Figure 3.13. VSFS spectra of ELP DV_2F-64 in the presence of deuterated solutions of 50 mM monovalent chloride salts at high pH. All experiments were performed with 1 mM tris buffer made in 99.9 % D_2O (pH 9.76). The spectra are offset by 0.4 units each for the sake of clarity.

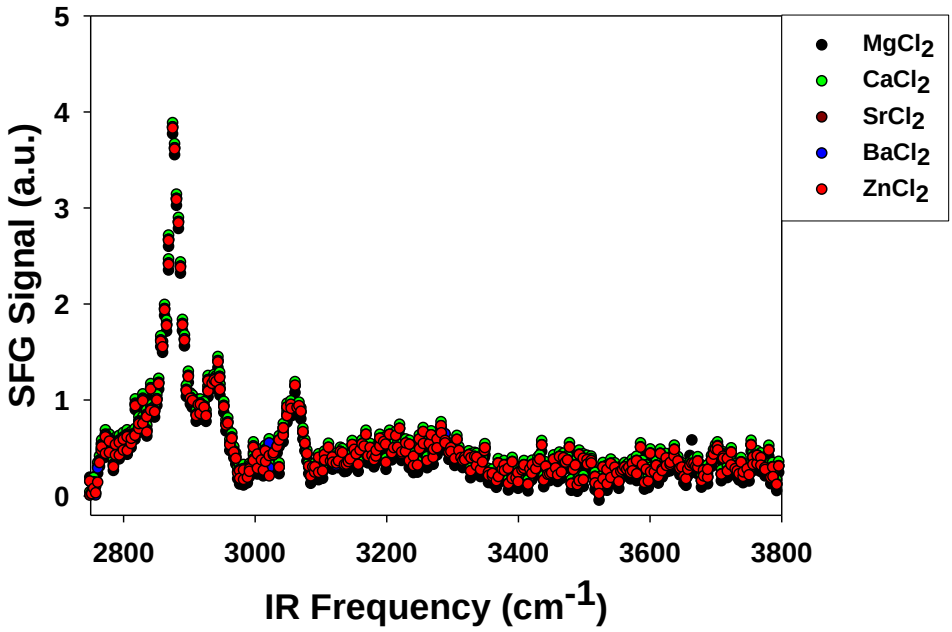

Figure 3.14. VSFS spectra of ELP DV_2F-64 in the presence of various divalent metal chloride salts at pH 2.7. All experiments were performed with 10 mM concentration of chloride salts in 1 mM tris buffer.

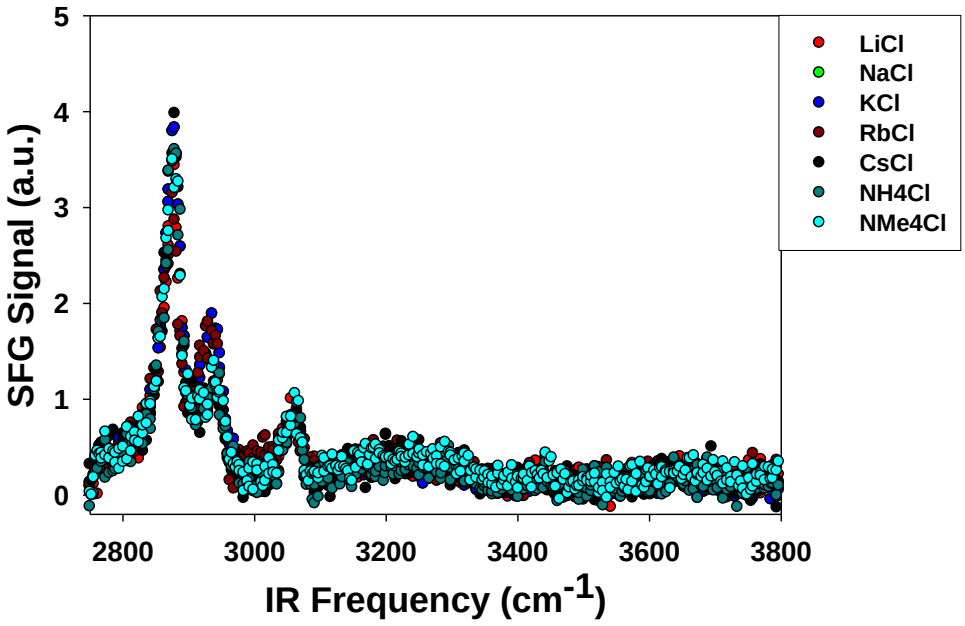

Figure 3.15. VSFS spectra of ELP DV_2F-64 in the presence of various monovalent metal chloride salts at pH 2.7. All experiments were performed with 10 mM concentration of chloride salts in 1 mM tris buffer.

Discussion

Effect of ions on the LCST of negatively charged ELPs

The thermodynamic data trends shown in Fig. 3.3 and Fig. 3.4 are in agreement with the partitioning tendencies of the monovalent and divalent metal ions found by using VSFS. These data demonstrate that the apparent dissociation constants for the divalent cations with the aspartate acid residues on the ELPs range from 1 mM to 8 mM (Table 3.1). On the other hand, the strongest binding monovalent alkali ion is Li^+ with an apparent dissociation constant of 280 mM. As such, even the smallest difference in affinity between a monovalent and divalent cation is a factor of 35 between Mg^{2+} and Li^+. On the other hand, Zn^{2+} has a dissociation constant which is 1250 times tighter than the $N(Me)_4^+$. The notion that divalent cations bind to acetate approximately two order of magnitude more tightly than monovalent cations is consistent with previous qualitative experiments describing the interactions of cations with negatively charged synthetic polyelectrolytes, peptides, nucleic acids and fatty acid headgroups.[78,80-85] Such strong interactions may also be a key reason for widespread presence of divalent cations in catalytic sites of numerous proteins and enzymes as well as their role in cell-signaling pathways and ligand-receptor binding events.[13,86-87]

Among the divalent ions, magnesium was found to show the weakest binding affinity to the carboxylate group (K_d = 8 mM). This is expected since magnesium is very strongly hydrated ion. As such, it should be energetically less favorable for magnesium to shed its hydration shells and form an ionic complex with aspartate.[88-89] The presence of very high charge density on the macromolecule may be a critical parameter for the

desolvation of magnesium ion in the binding process.[90] Binding of divalent ions becomes even more energetically favored in the presence of multiple aspartate or other negative charge residues.[91] Some calcifying species have been recently discovered to contain a very high concentration of negatively charged sites.[88] In fact, the amount of magnesium in biogenic calcites is controlled by the number of carboxylate-rich biomolecules.[90]

Historically, the solubility of various salts and their related hofmeister effects have been commonly explained using Collin's law of matching water affinities.[92-94] This idea predicts that the ions of similar hydration energies will be thermodynamically favored to form ion-pairs rather than staying as separate entities in the aqueous solutions. Some recent experimental and theoretical studies have also targeted understanding such ion-pairing affinities and their probable role in physiological phenomena such as the generation of ion gradients across cell membranes.[19,21,24,83,85,95-96] Based on this law, highly hydrated carboxylate side chains of proteins should have higher affinity towards similarly hydrated cations. This theory was quantitatively tested here by correlating the abstracted K_d values of each cation with the hydration enthalpy differences of acetate ion and cations (Fig. 3.16 and Fig. 3.17). Correlation was observed to be fairly good for monovalent cations, the only exceptions being Li^+ and NH_4^+ ions (Fig. 3.16). Na^+, as expected, was found to have stronger affinity for aspartate moiety as compared to potassium ion. Hydration energy of acetates and carboxylate groups are closer to Na^+ than to K^+. This preferential binding of sodium to the negatively charged acetate/carboxylate groups have been widely observed for very diverse macromolecular

systems such as proteins,[19,21,24] fatty acid headgroups,[23,95] polyelectrolytes,[97-98] mesoporous silica materials.[99] In the same order, chaotropic cations such as Rb^+ and Cs^+, on the other hand, are less favored to form stable ion-pairs with carboxylates. NH_4^+ was found to interact most strongly with the negatively charged aspartate moieties. This smaller K_d value is even more striking considering the fact that the pKa of NH_4^+ ion is 9.25. As a result, under the high pH experimental conditions (pH 9.76), the actual concentration of NH_4^+ was significantly less as compared to the conjugate base species NH_3 (1 mole of NH_4Cl produce approximately 0.24 moles of NH_4^+ and 0.76 moles of NH_3). NH_4^+ ions not only have the charge-driven favorable electrostatic affinity for the polypeptide carboxylates but also have the unique capability to form intramolecular and intermolecular hydrogen bonding in the multiple carboxylate residues containing polypeptides solutions.[100] This additional ionic association mechanism helps in bringing ELP chains closer and hence, a lower LCST value. Such types of opposite charged ion-ion associations and salt bridges are widely prevalent in folded protein structures and deemed very critical for their proper conformation and function. Tetramethyl ammonium ion, being most chaotropic, bound least effectively to the aspartate moieties. Unlike NH_4^+, it also lacks the capability to form hydrogen bonds.

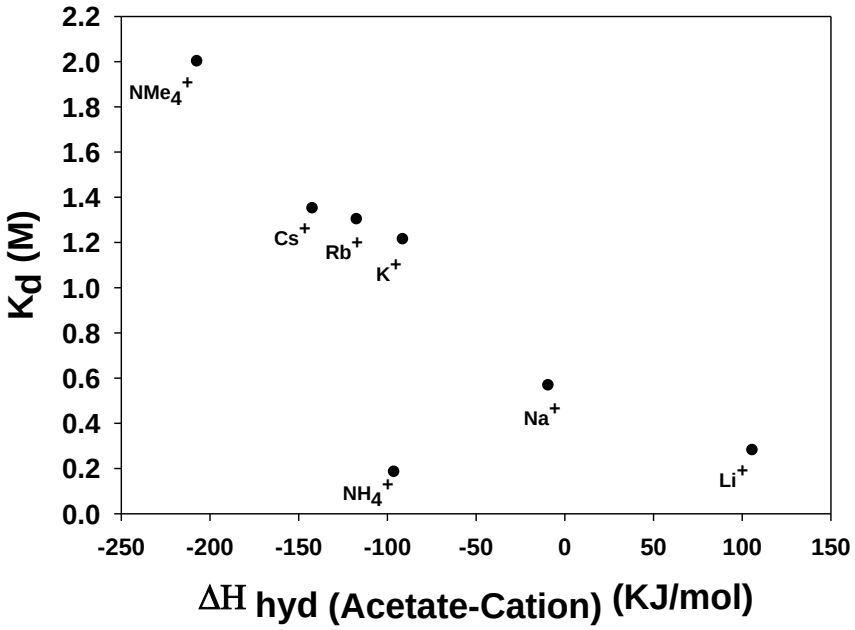

Figure 3.16. Correlation of observed K_d values with the standard hydration enthalpy difference between acetate ion and monovalent cation of each chloride salt.

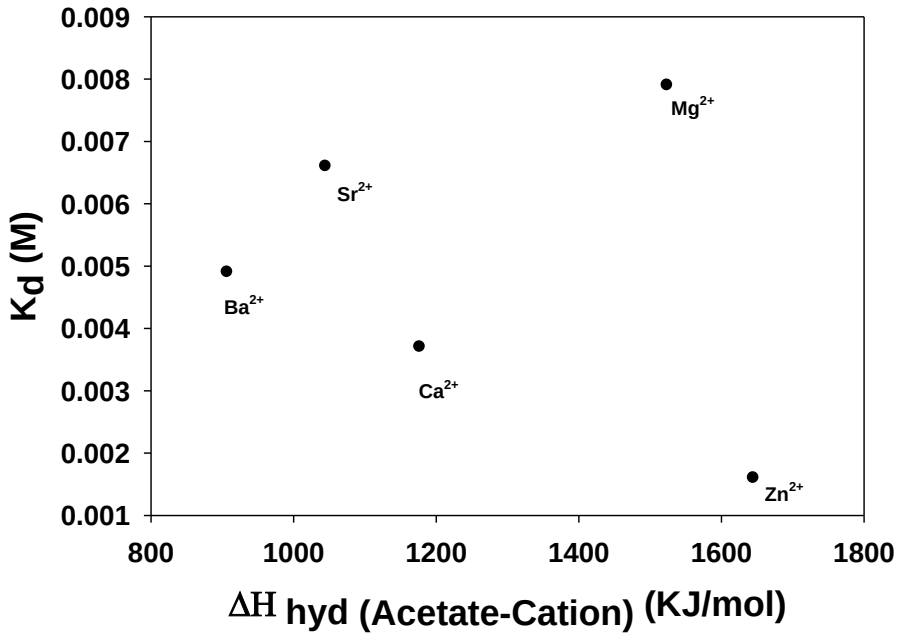

Figure 3.17. Correlation of observed K_d values with the standard hydration enthalpy difference between acetate ion and divalent cation of each chloride salt.

However, the corresponding correlation for divalent ions was found to be very poor (Fig. 3.17). Firstly, divalent ions despite having much larger hydration energies showed much stronger binding interactions with carboxylate groups (Table 3.2). Among the divalent cations themselves, Ba^{2+} has closest hydration energy as compared to acetate ion but it shows only intermediate binding efficiency. Zn^{2+}, on the other hand, showed the highest preference for carboxylate anion despite having the largest hydration energy barrier. As we have clearly demonstrated here, these specific ion-pairing interactions cannot be simply explained in terms of their respective hydration properties only. The exact chemical nature of ion-pairing,[24,101] presence of d-orbitals in transition metals, availability of multiple binding sites and its influence on more favorable carboxylate binding modes and its impact on ion specificity should be taken into account. [87,90-91,102] Previously, it has also been shown that the surface tension of metal chloride solutions stays almost the same irrespective of the chemical identity of cationic species (Table 2.2). Hence, the possible role of surface tension effects in the observed cation preferences, especially at low concentrations, can be safely ruled out. This is in stark contrast to much larger differences observed in the surface tension values of various hofmeister anions.[56] Not surprisingly, these surface tension variations have been cited as one of the major factors determining the overall ordering of anions in Hofmeister series and their dominance over cations in affecting the protein solubility in solutions.[15,58]

Table 3.2. Enthalpy of hydration values of different cations and their comparison with hydration affinity of an acetate ion.[57]

Ion	**ΔH_{hydr} (KJ/mol)**	**$\Delta H_{hydr(acetate\text{-}cation)}$ (KJ/mol)**
Li^+	-531	106
Na^+	-416	-9
K^+	-334	-91
Rb^+	-308	-117
Cs^+	-283	-142
NH_4^+	-329	-96
NMe_4^+	-218	-207
Mg^{2+}	-1949	1524
Ca^{2+}	-1602	1177
Sr^{2+}	-1470	1045
Ba^{2+}	-1332	907
Zn^{2+}	-2070	1645

* Enthalpy of hydration value for acetate ion is -425 KJ/mol.

Large orders of magnitude of differences observed in K_d values of monovalent and divalent ions as compared to rather small variations in their *c* values also supports our viewpoint that cation specificity is induced by these binding interactions to aspartate groups. It should also be noted that the multiple phenylalanine residues present in the polypeptide could potentially play a role in cation partitioning to the protein surface via cation-π interactions.[103-104] However, such interactions are known to be substantially weaker than the ion pairing interactions and becomes even more attenuated when the ions are freely mobile and solvated.[105-106] In the VSFS experiments performed at the air-water interface, the hydrophobic phenylalanine moieties should largely be pointing upward into the air and as such are not available for binding with the cations. The lack of ion specificity under protonated conditions in Figs. 3.14 and 3.15 are a good indication that the all ion specificity measured by VSFS comes from the deprotonated acetates as pH changes would be expected to have less influence on cation-π effects. LCST measurements done at low pH also confirmed this hypothesis (Fig. 3.7). Apart from the hydrophobic moieties and amide backbone, phenylalanine residues and protonated aspartate residues could be thought of as the only putative binding sites for cations under such conditions. However, the LCST decrease was insignificantly small and mostly non-specific and exponential binding part was missing. Therefore, specific cation partitioning to the charged polypeptide surface is primarily driven by very strong interactions of cations with deprotonated acidic residues rather than the much weaker, if any, interactions with phenylalanine residues.

Conclusions

In conclusion, vital role of carboxylate-cation interactions in inducing cation specificity was highlighted in this particular study. Cations, in general, prefer to stay solvated in the bulk solution and tend to be excluded from uncharged, hydrophobic protein surfaces (Chapter II).[6] This behavior of cations is dramatically different from those of anions. Infact, chaotropic anions have previously been shown to have tendency to accumulate and interact with hydrophobic air-water and protein surfaces.[15,50] Absence of any preferential association of cations with protein-like polymeric interface also hints at the lack of affinity of cations to interact with hydrophobic or polar amide group atleast under physiologically relevant salt concentrations. Proteins having multiple acidic residues, however, have a significant negative surface potential. This results in formation of thermodynamically favorable contact ion-pairs or solvent separated ion pairs. Divalent ions show much stronger binding affinities to the aspartate residues as compared to less charged monovalent ions.

CHAPTER IV

CONCLUSIONS

Elastin-like polypeptides are a very simple and effective model system for investigating specific cation interactions observed in various physiologically relevant processes such as protein folding/aggregation, enzyme activity, signal transduction via ion-channels. These polypeptides can be easily engineered to obtain non-polar, polar, charged sequences for studying the relative role and importance of different protein motifs in inducing cation selectivity and specificity.[29] Another model biopolymeric system, poly(*N*-isopropylacrylamide), is also successfully used here to compliment the studies done with ELPs.

First, specific cation effects on the phase transition temperature of a neutral ELP and PNIPAM were investigated for a series of alkali, alkaline-earth metal and transition metal chloride solutions. Dominant role of anionic species (i.e. chloride ion) was clearly seen in salt solutions of these neutral, uncharged biopolymers. However, some differences in cation specificities were also observed. The trends followed a direct hofmeister series. Smaller alkali cations such as Na^+ and K^+ salted-out biopolymers more effectively. In contrast, larger, more polarizible ions such as Rb^+ and Cs^+ had lesser effect on LCST values of ELPs/PNIPAM. Dispersion interactions of these ions with the hydrophobic side chains of ELP/PNIPAM help in biopolymer solubilization and hence, lesser salting-out effect of chloride species. Highly hydrated, charged ions like Li^+ and divalent ions, had lesser salting-out constants for a different reason. These ions

are less depleted from biopolymer surfaces and presumably show a weak, indirect binding affinity for carbonyl groups of amide moieties through their hydration shell.

Very strong cation preferences and selectivities are, however, commonly observed in biological systems at significantly lower salt concentrations (< 500 mM).[13] Role of negatively charged acidic amino acids residues in inducing these specific cation preferences was successfully demonstrated using a genetically engineered aspartate-rich ELP. Surface-sensitive spectroscopy measurements coupled with phase transition temperature data of this ELP conclusively proved the huge importance of charged groups on protein surfaces in driving these cation preferences. Detailed quantitative and qualitative information of ion-paring affinities between carboxylate residues and cations were obtained. Divalent cations showed a much stronger affinity for carboxylate groups as compared to monovalent cations. Additionally, it was proven that the association between counter ions can not be simply viewed as a favorable pairing of two similarly hydrated anionic and cationic groups. Amount of charge on the protein surface, chemical identity of the charged groups, and availability of d-orbitals and complexation ability of different metal ions indeed plays a vital role in determining this significant preference of one cation over another. Once the negative charge on the biopolymer surface is neutralized, much weaker salt interactions take place. These includes the dominant surface tension effect of anions and weak dispersion forces of cations and even weaker interactions of cations with carbonyl group of amide moiety.

REFERENCES

(1) Hofmeister, F. *Arch Exp Pathol Pharmakol* **1888**, *24*, 247-260.

(2) Kunz, W.; Lo Nostro, P.; Ninham, B. W. *Curr. Opin. Coll. Int. Sci.* **2004**, *9*, 1-18.

(3) Kunz, W.; Henle, J.; Ninhan, B. W. *Curr. Opin. Coll. Int. Sci.* **2004**, *9*, 19-37.

(4) Collins, K. D.; Washabaugh, M. W. *Q. Rev. Biophys.* **1985**, *18*, 323-422.

(5) Baldwin, R. L. *Biophys. J.* **1996**, *71*, 2056-2063.

(6) Cacace, M. G.; Landau, E. M.; Ramsden, J. J. *Q. Rev. Biophys.* **1997**, *30*, 241-277.

(7) Zhang, Y.; Cremer, P. S. *Curr. Opin. Chem. Biol.* **2006**, *10*, 658-663.

(8) Petersen, P. B.; Saykally, R. J. *Annu Rev Phys Chem* **2006**, *57*, 333-364.

(9) Traube, J. *J. Phys. Chem.* **1910**, *14*, 452-470.

(10) Zhang, Y.; Cremer, P. S. *Ann. Rev. Phys. Chem.* **2010**, *61*, 63-83.

(11) Nostro, P. L.; Fratoni, L.; Ninham, B. W.; Baglioni, P. *Biomacromolecules* **2002**, *3*, 1217-1224.

(12) Ganguly, P.; Schravendijk, P.; Hess, B.; van der Vegt, N. F. A. *J. Phys. Chem. B* **2011**, *115*, 3734-3739.

(13) Stryer, L. *Biochemistry*, 4th Ed.; W. H. Freeman and Co.: New York, 1995.

(14) Omta, A. W.; Kropman, M. F.; Wountersen, S.; Bakker, H. J. *Science* **2003**, *301*, 347-349.

(15) Zhang, Y. J.; Furyk, S.; Bergbreiter, D. E.; Cremer, P. S. *J. Am. Chem. Soc.* **2005**, *127*, 14505-14510.

(16) Lund, M.; Vrbka, L.; Jungwirth, P. *J. Am. Chem. Soc.* **2008**, *130*, 11582-11583.

(17) Zhang, Y. J.; Furyk, S.; Sagle, L. B.; Cho, Y.; Bergbreiter, D. E.; Cremer, P. S. *J. Phys. Chem. C* **2007**, *111*, 8916-8924.

(18) Cho, Y.; Zhang, Y.; Christensen, T.; Sagle, L.; Chilkoti, A.; Cremer, P.S. *J. Phys. Chem. B* **2008**, *112*, 13765-13771.

(19) Vrbka, L.; Vondrášek, J.; Jagoda-Cwiklik, B.; Vácha, R.; Jungwirth, P. *Proc. Natl. Acad. Sci. U. S. A.* **2006**, *103*, 15440-15444.

(20) Heyda, J.; Pokorna, J.; Vrbka, L.; Vacha, R.; Jagoda-Cwiklik, B.; Konvalinka, J.; Jungwirth, P.; Vondrasek, J. *Phys. Chem. Chem. Phys.* **2009**, *11*, 7599-7604.

(21) Jagoda-Cwiklik, B.; Vácha, R.; Lund, M.; Srebro, M.; Jungwirth, P. *J. Phys. Chem. B* **2007**, *111*, 14077-14079.

(22) Tang, C.Y.; Allen, H. C. *J. Phys. Chem. A.* **2009**, *113*, 7383-7393.

(23) Jäger, C. M.; Hirsch, A.; Schade, B.; Bötcher, C.; Clark, T. *Chem.─ Eur. J.* **2009**, *15*, 8586-8592.

(24) Hess, B.; van der Vegt, N. F. A. *Proc. Natl. Acad. Sci. U. S. A.* **2009**, *106*, 13296-13300.

(25) Von Hippel, P. H.; Peticolas, V.; Schack, L.; Karlson, L. *Biochemistry* **1973**, *12*, 1256-1264.

(26) Boström, M.; Williams, D. R. M.; Ninham, B. W. *Biophys. J.* **2003**, *85*, 686-694.

(27) Heskins, M.; Guillet, J.E. *J. Macromol. Sci.* **1968**, *2*, 1441-1455.

(28) Schild, H.G. *Prog. Polym. Sci.* **1992**, *17*, 163-249.

(29) Meyer, D. E; Chilkoti, A. *Biomacromolecules* **2002**, *3*, 357-367.

(30) Meyer, D.E.; Chilkoti, A. *Biomacromolecules* **2004**, *5*, 846-851.

(31) Flamia, R.; Zhdan, P.A.; Martino, M.; Castle, J.E.; Tamburro, A.M. *Biomacromolecules* **2004**, *5*, 1511-1518.

(32) Ohgo, K.; Ashida, J.; Kumashiro, K.K.; Asakura, T. *Macromolecules* **2005**, *38*, 6038-6047.

(33) Kumashiro, K.K.; Kurano, T.L.; Niemczura, W.P.; Martino, M.; Tamburro, A.M. *Biopolymers* **2003**, *70*, 221-226.

(34) Ohgo, K.; Kurano, T.L.; Kumashiro, K.K.; Asakura, T. *Biomacromolecules* **2004**, *5*, 744-750.

(35) Yao, X.L; Hong, M.J. *J. Am. Chem. Soc*. **2004**, *126*, 4199-4210.

(36) Schmidt, P.; Dybal, J.; Rodriguez-Cabello, J.C.; Reboto, V. *Biomacromolecules* **2005**, *6*, 697-706.

(37) Li, B.; Alonso, D.O.V.; Bennion, B.J.; Daggett, V. *J. Am. Chem. Soc*. **2001**, *123*, 11991-11998.

(38) Operation and Service Manual: *MPA100 Optimelt Automated Melting Point System*; Stanford Research Systems: California, 2006.

(39) Shen, Y. R. *Nature* **1989**, *337*, 519-525.

(40) Shen, Y. R. *The Principles of Nonlinear Optics*; John Wiley & Sons: New York, 1984.

(41) Richmond, G. L. *Chem. Rev.* **2002**, *102*, 2693-2724.

(42) Liu, J.; Conboy, J. C. *J. Am. Chem. Soc.* **2004**, *126*, 8376-8377.

(43) Shen, Y. R.; Ostroverkhov, V. *Chem. Rev.* **2006**, *106*, 1140-1154.

(44) Nagata, Y.; Mukamel, S. *J. Am. Chem. Soc.* **2010**, *132*, 6434-6442.

(45) Chen, X.; Hua, W.; Huang, Z.; Allen, H. C. *J. Am. Chem. Soc.* **2010**, *132*, 11336-11342.

(46) Kim, J.; Cremer, P. S. *J. Am. Chem. Soc.* **2000**, *122*, 12371-12372.

(47) Tiktopulo, E.I.; Uversky, V.N.; Lushchik, V.B.; Klenin, S.I.; Bychkova, V.E.; Ptitsyn, O.B. *Macromolecules* **1995**, *28*, 7519-7524.

(48) Furyk, S.; Zhang, Y.; Acosta, D.O.; Cremer, P.S; Bergbreiter, D.E. *J. Poly. Sci.*: *Part A* **2006**, *44*, 1492-1501.

(49) Meyer, D. E.; Chilkoti, A. *Nat. Biotechnol.* **1999**, *17*, 1112–1115.

(50) Chen, X.; Yang, T. L.; Kataoka, S.; Cremer, P. S. *J. Am. Chem. Soc.* **2007**, *129*, 12272-12279.

(51) Chen, X.; Flores, S. C; Lim, S. M.; Zhang, Y.; Yang, T.; Kherb, J.; Cremer, P. S. *Langmuir* **2010**, *26*, 16447-16454.

(52) Jarvis, N. L.; Scheiman, M. A. *J. Phys. Chem.* **1972**, *72*, 74-78.

(53) Hrobarik, T.; Vrbka, L.; Jungwirth, P. *Biophys. Chem.* **2006**, *124*, 238-242.

(54) Pegram, L. M.; Record, M. T., Jr. *Chem. Phys. Lett.* **2008**, *467*, 1-8.

(55) Pegram, L. M.; Record, M. T., Jr. *J. Phys. Chem. B* **2008**, *112*, 9428-9436.

(56) Weissenborn, P. K.; Pugh, R. J. *J. Coll. Inter. Sci.* **1996**, *184*, 550-563.

(57) Marcus, Y. *Ion Properties*; Marcel Dekker: New York, 1997.

(58) Pegram, L. M.; Record, M. T., Jr. *J. Phys. Chem. B* **2007**, *111*, 5411-5417.

(59) Debye, P.; McAulay, *J. Phys. Z.* **1925**, *26*, 22-29.

(60) Long, F. A.; McDevit, W. F. *Chem. Rev.* **1952**, *51*, 119-169.

(61) McDevit, W. F.; Long, F. A. *J. Am. Chem. Soc.* **1952**, *74*, 1773-177.

(62) Masterton, W. L.; Lee, T. P. *J. Phys. Chem.* **1970**, *74*, 1776-1782.

(63) Breslow, R.; Guo, T. *Proc. Natl. Acad. Sci. U. S. A.* **1990**, *87*, 167-169.

(64) Freitag, R.; Garrett-Flaudy, F. *Langmuir* **2002**, *18*, 3434-3440.

(65) Robinson, D. R.; Jencks, W. P. *J. Am. Chem. Soc.* **1965**, *87*, 2470-2479.

(66) Nandi, P. K.; Robinson, D. R. *J. Am. Chem. Soc.* **1972**, *94*, 1299-1308.

(67) Nandi, P. K.; Robinson, D. R. *J. Am. Chem. Soc.* **1972**, *94*, 1308-1315.

(68) Diamond, R. M. *J. Phys. Chem.* **1963**, *67*, 2513-2517.

(69) Desnoyers, J. E.; Pelletier, G. E.; Jolicoeur, C. *Can. J. Chem.* **1965**, *43*, 3232-3237.

(70) Wolff, J.; Sackett, D. L.; Knipling, L. *Pro. Sci.* **1996**, *5*, 2020-2028.

(71) Ikegami, A.; Imai, N. *J. Poly. Sci.* **1962**, *56*, 133-152.

(72) Gregor, H. P.; Hamilton, M. J.; Oza, R. J.; Bernstein, F. *J .Phys. Chem.* **1956**, *60*, 263-267.

(73) Newman, J. K.; McCormick, C. L. *Macromolecules* **1994**, *27*, 5114-5122.

(74) Strauss, U. P.; Leung, Y. P. *J. Am. Chem. Soc.* **1965**, *87*, 1476-1480.

(75) Nagata, I.; Okamoto, Y. *Macromolecules* **1983**, *16*, 749-753.

(76) Sabbagh, I.; Delsanti, M. *Eur. Phys. J. E* **2000**, *1*, 75-86.

(77) Shkol'nikov, E. V. *Russ. J. Appl. Chem.* **2004**, 77, 1255-1258.

(78) Gurau, M. C.; Kim, G.; Lim, S. M.; Albertorio, F.; Fleisher, H. C.; Cremer, P. S. *Chem. Phys. Chem.* **2003**, *4*, 1231-1233.

(79) Zhang, Y.; Cremer, P. S. *Proc. Natl. Acad. Sci. U. S. A.* **2009**, *106*, 15249-15253.

(80) Manning, G. S. *Q. Rev. Biophys.* **1978**, *11*, 179-246.

(81) Begala, J. A.; Strauss, U. P. *J. Phys. Chem.* **1972**, *76 (2)*, 254-260.

(82) Bulo, R. E.; Donadio, D.; Laio, A.; Molnar, F.; Rieger, J.; Parrinello, M. *Macromolecules* **2007**, *40*, 3437-3442.

(83) Mattai, J.; Kwak, J. C. T. *Macromolecules* **1986**, *19*, 1663-1667.

(84) Gustafson, R. L.; Lirio, J. A. *J. Phys. Chem.* **1968**, *72*, 1502-1505.

(85) Tang, C. Y.; Huang, Z.; Allen, H. C. *J. Phys. Chem. B* **2011**, *115*, 34-40.

(86) Dudev, T.; Lim, C. *Chem. Rev.* **2003**, *103*, 773-787.

(87) Babu, C. S.; Dudev, T.; Casareno, R.; Cowan, J. A.; Lim, C. *J. Am. Chem. Soc.* **2003**, *125*, 9318-9328.

(88) Stephenson, A. E.; DeYoreo, J. J.; Wu, L.; Wu, K. J.; Hoyer, J.; Dove, P. M. *Science* **2008**, *322*, 724-727.

(89) Addadi, L.; Weiner, S. *Proc. Natl. Acad. Sci. U. S. A.* **1985**, *82*, 4110-4114.

(90) Wang, D.; Wallace, A. F.; De Yoreo, J. J.; Dove, P. M. *Proc. Natl. Acad. Sci. U. S. A.* **2009**, *106*, 21511-21516.

(91) Dudev, T.; Carmay, L. *Acc. Chem. Res.* **2007**, *40*, 85-93.

(92) Collins, K. D. *Proc. Natl. Acad. Sci. U. S. A.* **1995**, *92*, 5553-5557.

(93) Collins, K. D. *Methods* **2004**, *34*, 300-311.

(94) Collins, K. D.; Neilson, G. W.; Enderby, J. E. *Biohys. Chem.* **2007**, *128*, 95-104.

(95) Vlachy, N.; Jagoda-Cwiklik, B..; Vacha, R.; Touraud, D.; Jungwirth, P.; Kunz, W. *Adv. Coll. Int. Sci.* **2009**, *146*, 42-47.

(96) Vácha, R.; Jurkiewicz, P.; Petrov, M.; Berkowitz, M. L.; Böckmann, R. A.;

Barucha-Kraszewska, J.; Hof, M.; Jungwirth, P. *J. Phys. Chem. B* **2010**, *114*, 9504-9509.

(97) Tondre, C.; Zana, R. *J. Phys. Chem.* **1971**, *75*, 3367-3372.

(98) Zana, R.; Tondre, C.; Rinaudo, M.; Milas, M. *J. Chim. Phys. Physiochem. Biol.* **1971**, *68*, 1258-1261.

(99) Salis, A.; Parsons, D. F.; Bostrőm, M.; Medda, L.; Barse, B.; Ninham, B. W.; Monduzzi, M. *Langmuir* **2010**, *26*, 2484-2490.

(100) Sada, K.; Tani, T.; Shinkai, S. *Synlett* **2006**, *15*, 2364-2374.

(101) Marcus, Y.; Hefter, G. *Chem. Rev.* **2006**, 106, 4585-4621.

(102) Ryde, U. *Biophys. J.* **1999**, *77*, 2777-2787.

(103) Dougherty, D. A. *Science* **1996**, *271*, 163-168.

(104) Gallivan, J. P.; Dougherty, D. A. *Proc. Natl. Acad. Sci. U. S. A.* **1999**, *96*, 9459-9464.

(105) Reddy, A. S.; Zipse, H.; Sastry, G. N. *J. Phys. Chem. B* **2007**, *111*, 11546-11553.

(106) Rao, J. S.; Zipse, H.; Sastry, G. N. *J. Phys. Chem. B* **2009**, *113*, 7225-7236.

VITA

Name: Jaibir Kherb

Address: Department of Chemistry, Texas A&M University, Texas, USA

Email Address: jkherb@mail.chem.tamu.edu

Education: B.S., Chemistry (Honors), University of Delhi, Delhi, India, 2003

M.S., Chemistry, Indian Institute of Technology-Delhi, India, 2006

Ph.D. Chemistry, Texas A&M University, Texas, USA, 2011